

We thank the instructive and detail points given by the two reviewers. We have carefully revised our manuscript accordingly. Below is our point-to-point response.

Reviewer1:

Reviewer: Bian et al. compare global nitrate and ammonium budgets for 9 global chemical models in order to assess differences between the models and attribute these differences to specific processes. This is part of the AeroCom Phase III study. They find that burdens of HNO₃ and NO₃⁻ differ by factors of 9 and 13, respectively, between the different models. The modeled differences in the NH₃/NH₄⁺ burdens were unclear and should be explicitly stated. Modeled chemical production of NH₄⁺ and lifetime differed by factors of 2 and 5, respectively. They attribute these model differences to differences in 1) pH-dependent wet deposition of NH₄⁺, 2) nitrate formation on the surface of sea salt and dust aerosol, and 3) the nitrate coarse mode fraction. They find that nitrate production on sea salt and dust is important to include in models as it tends to dominate nitrate production and controls its partitioning between the fine and coarse mode. In that sense it seems to me that 2 and 3 above are referring to the same process. They also compare the model results to observations of nitrate and ammonium surface observations of concentrations and deposition, as well as observed vertical profiles from several aircraft campaigns.

Authors: A sentence that describes the differences in the NH₃/NH₄⁺ burdens is added right after the description for HNO₃ and NO₃ in the abstract (lines 38-39). We intend to separate discussion of section 5.2 and 5.3 because the nitrate formation on the surface of sea salt and dust aerosol (section 5.3) is important, but not the only factor, to determining nitrate size distribution (section 5.2). Also, the former focuses more on chemical process and the later on physical process and climate implication.

Reviewer: Overall this is a well written paper and will be useful for assessing reactive nitrogen budgets in models. One thing I found confusing was the use of the phrase “heterogeneous chemistry” and the use of the term “nitrate”. For me, when I hear heterogeneous chemical production of nitrate I think of N₂O₅ hydrolysis, which this paper did not examine at all. I wonder how nitrate production from N₂O₅ hydrolysis differs in the models and if this can account for some of the inter-model variability. There was no mention at all of model differences in nitrate production (NO₂+OH, BrONO₂ hydrolysis, etc) and how this might account for model differences. Perhaps this will be the subject of another paper, and if so it would be nice to mention that here. What the authors are referring to by the use of “heterogeneous chemistry” is what I would call thermodynamic partitioning between the gas and aerosol phase. Perhaps the authors should reconsider their choice of words here so that it is not confusing. Also, when I read “nitrate” I think of HNO₃(g) + NO₃⁻, i.e., the sum of gas and particulate nitrate. In this paper, “nitrate” is specifically referring to the particulate phase. Perhaps use the term “particulate nitrate” or “NO₃⁻” instead so it is more clear. That might also partially help with the issue above regarding the term heterogeneous chemistry.

Authors: We add a sentence “hereafter nitrate referring to particulate nitrate unless otherwise specified” in the introduction (line 56). We also add the following clarification in section 2.2 (lines 216-220). “Please also note that the heterogeneous chemical production of nitrate mentioned in this paper refers only the reaction of HNO₃ on dust and sea salt particles. A series of reactions, such as N₂O₅ hydrolysis and BrONO₂ hydrolysis, affect

HNO₃ simulation. These reactions are typically considered in O₃-NO_x-HO_x chemistry and their discussion is beyond the scope of this paper.”

More minor issues:

Lines 363 and 364 need subscripts.

Authors: Done.

Line 460: replace “decease” with “decrease”

Authors: Done.

Line 539: What does “the correction of pH in cloud water” mean? It sounds like the models are somehow correcting for a cloud pH calculation. If I understand correctly, it is not the pH calculation that is being corrected, but whether or not pH is being considered in the Henry’s law constant calculation for NH₃.

Authors: Delete “correction of” before pH.

Line 569: Check the grammar

Authors: The sentence has been revised to be “The latter corresponds to a range of pH from 4.5 (Oslo-CTM2) to 5.5 (CHASER).”

Paragraphs beginning on lines 743 and 761 should be combined for clarity.

Authors: Yes, combined now.

Line 785: “model” should read “mode”

Authors: Done.

Reviewer2:

Reviewer: This paper presents results from 9 global models with a focus on nitrate aerosol. Since nitrate aerosol formation is linked to ammonia, ammonium, sulfate, and nitric acid, additional species and their deposition is also evaluated. The authors provide insight into the model differences by noting which models include heterogeneous chemistry and pH depending NH₃ solubility (Henry’s Law). I have one major comment and other minor comments.

Major comment:

At the end of the paper, it is not clear what processes or species future model development should target to improve nitrate aerosol formation. Some insight may be gained by more carefully considering how errors in sulfate (and ammonium) may propagate to errors in aerosol nitrate. In particular, the correlation between model predictions and observations for NH₄ and SO₄ is quite poor for some models (Figure 4). Consider Weber et al. (2016) and how decreases in sulfate do not necessarily lead to decreases in aerosol H⁺ (in contrast to page 2, lines 78-80). As nitrate partitioning is sensitive to pH, nitrate aerosol formation could be limited due to aerosol pH. Weber et al. (2016) and Silvern et al. (2017) have indicated pH may decrease (aerosols become more acidic) in the future. Can the limiting factor (NH₃, nitrate, or pH) for nitrate formation be better identified?

Authors: Thanks to the reviewer for bringing this insightful point to the discussion of potential future study. We have expanded the discussion in the conclusion (lines 814-839).

“Our work presents a first effort to assess nitrate simulation from chemical and physical processes. A companion study is proposed by AeroCom III nitrate activity to investigate how sensitive is nitrate formation in response to the possible future changes of emission and meteorological fields. These perturbation fields include increasing NH_3 emission, decreasing NO_x , SO_x and dust emissions, and increasing atmospheric temperature and relative humidity. **It would be particularly interesting to examine how aerosol pH changes and its influence on atmospheric acid/base gas-particle system during the experiment. Future aerosol pH does not necessarily increase with SO_2 emission reduction. Indeed, studies over US southeast indicated that its aerosol has been getting more acidic over the past decade although SO_2 emission decreased and NH_3 emission stayed constant [Silvern et al., 2017; Weber et al., 2016]. This environment of high aerosol acidity hinders the formation of nitrate aerosol, which only occurs when pH is over ~ 2 to 3 [Weber et al., 2016]. In addition, understanding why and how the system is insensitive to changing SO_2 level due to buffering of the partitioning of semivolatile NH_3 over regions such as US southeast helps us to gain some insight into how errors in sulfate (and ammonium) may propagate to errors in aerosol nitrate. In particular, the correlation between model predictions and observations for SO_4^{2-} and NH_4^+ is quite poor for some models (Figure 4). It would be also interesting to include organic gas/aerosol into the system since they are not only important atmospheric components, but also reduce the uptake of NH_3 . Competition for uptake between NH_3 and organic gases considerably slows down the approach to thermodynamic equilibrium [Silvern et al., 2017].** Based on the findings of this work, modelers should pay particular attention to incorporating dust and sea salt and treating NH_3 wet deposition to improve nitrate simulation. Further evaluation using satellite measurements, such as NH_3 products from IASI and TES, is desired and will be conducted. Such evaluation requires global 3-dimensional high frequency model data. Potential future study also includes estimation of nitrate forcing for climate change.”

By the way, the sentence in original submission page 2 lines 78-80 just states the facts of abundant NO_3 and SO_4 observed in atmosphere.

Minor comments:

1. The authors should carefully check for awkward wording

Authors: Yes. We have also revised the manuscript based at the reviewers' suggestion.

2. Line 154: reword to “emission inventories used”

Authors: Done.

3. Line 186: Was the several months of spinup for meteorology and chemistry or just meteorology? Is several months sufficient for chemistry of the upper troposphere?

Authors: The spinup period is for chemistry simulation. We have changed “several months” to “one-year” as specified in the protocol of AeroCom III nitrate experiment. One-year of spinup should be fine for the chemical species discussed in this study in the upper troposphere.

4. Line 204: Can the differences in organic nitrate treatments be briefly discussed? It would be useful to have production rates of nitric acid from each model.

Authors: Although gas- and aerosol-phase organic nitrates are important, the chemistry formation and degradation remains uncertain [Fisher et al., 2016]. To my knowledge, the models involved in this experiment do not have aerosol-phase organic nitrate. We agree with the reviewer on the usefulness of having production rates of nitric acid from each model. We specified this requirement in the experiment protocol. Unfortunately only two

models submitted this kind of data, which were presented in our table 4c.

Fisher, J. A., Jacob, D. J., Travis, K. R., Kim, P. S., Marais, E. A., Chan Miller, C., Yu, K., Zhu, L., Yantosca, R. M., Sulprizio, M. P., Mao, J., Wennberg, P. O., Crouse, J. D., Teng, A. P., Nguyen, T. B., St. Clair, J. M., Cohen, R. C., Romer, P., Nault, B. A., Wooldridge, P. J., Jimenez, J. L., Campuzano-Jost, P., Day, D. A., Hu, W., Shepson, P. B., Xiong, F., Blake, D. R., Goldstein, A. H., Miszta, P. K., Hanisco, T. F., Wolfe, G. M., Ryerson, T. B., Wisthaler, A., and Mikoviny, T.: Organic nitrate chemistry and its implications for nitrogen budgets in an isoprene- and monoterpene-rich atmosphere: constraints from aircraft (SEAC4RS) and ground-based (SOAS) observations in the Southeast US, *Atmos. Chem. Phys.*, 16, 5969-5991, <https://doi.org/10.5194/acp-16-5969-2016>, 2016.

5. Line 225: Are solid precipitates allowed in any of the metastable configurations?

Authors: No. For a metastable configuration, aerosol is composed only of an aqueous phase that can be supersaturated with respect to dissolved salts.

6. Line 256: typo ISORROPIA-I

Authors: Done.

7. Line 528-520: sentence is unclear

Authors: Change the sentence to “Consequently, the slopes of the fitting lines are generally less than 1 on the scattering plots with model as y-axis and observation as x-axis (e.g. Figures 4a-d, 6, 7a-b).”

8. Line 619: Is the goal to compromise accuracy and efficiency?

Authors: Yes.

9. Line 731: Can you clarify what fraction actually used the HTAP2 emission inventory vs something else?

Authors: The detailed discussion for the fraction actually used the HTAP2 emission inventory is presented in section 2.1. We have added “for aerosol and ozone simulations” after “Emissions from anthropogenic, aircraft, and ship” on line 171. We have also added “for the aerosol and gas emissions from anthropogenic, aircraft, and ship sources” after “use HTAP2 emission inventory” on lines 738-739.

10. Line 753: Do you mean ammonium measured on filters?

Authors: Yes.

11. Line 782: Is it thus possible to recommend that all models use the pH dependent Henry’s law coefficient for NH₃? Can other recommendations for models be succinctly stated in the conclusions?

Authors: Since liquid-phase reaction 2 in Appendix can reach equilibrium quickly within a chemical time step, we recommend including it in accounting for NH₃ solution. Theoretically, a more accurate approach is to combine wet removal with liquid-phase chemistry calculation. In other words, instead of using an implicit calculation of the effective Henry’s law constant, the gas-liquid phase equilibrium is explicitly calculated based on the chemical mechanism used in the liquid phase. The solution of NH₃ is calculated by solving a set of partial differential equations, which includes not only the gas-liquid phase equilibrium, but also all the important reactions in the liquid phase, as adopted in EMAC model. We have added this discussion in the conclusion (lines 788-796).

12. Table 1: Define CHEMDUSS (not defined until later table)

Authors: Done

13. Figure 5: Why are the daily and monthly output results (Figure 5) so different? For the daily output, is the aircraft data matched on a daily basis?

Authors: The big difference between the daily and monthly output is mainly shown by the ATCTAS April campaign. The April experiment was conducted over Alaska for long-range transport of Asia pollution so that the day-to-day atmospheric dynamic variation could play more on the pollution over Alaska. For the daily output, the model and aircraft data match on a daily basis.

14. Make sure abbreviations are defined in the tables (for example CheAP in 4c and ChemGP in 4d)

Authors: Done.

Investigation of global nitrate from the AeroCom Phase III experiment

Huisheng Bian^{1,2}, Mian Chin², Didier A. Hauglustaine³, Michael Schulz⁴, Gunnar Myhre^{5,6},
Susanne E. Bauer^{7,8}, Marianne T. Lund⁶, Vlassis A. Karydis⁹, Tom L. Kucsera¹⁰, Xiaohua Pan¹¹,
Andrea Pozzer⁹, Ragnhild B. Skeie⁶, Stephen D. Steenrod¹⁰, Kengo Sudo¹², Kostas
Tsigaridis^{7,8}, Alexandra P. Tsimpidi⁹, and Svetlana G. Tsyro⁴

¹ Joint Center for Environmental Technology UMBC, Baltimore, MD, USA

² Laboratory for Atmospheres, NASA Goddard Space Flight Center, Greenbelt, MD, USA

³ Laboratoire des Sciences du Climat et de l'Environnement (LSCE), UMR8212, CEA-CNRS-UVSQ, Gif-sur-Yvette, France

⁴ Norwegian Meteorological Institute, Blindern, Norway

⁵ Department of Geosciences, University of Oslo, Oslo, Norway

⁶ Center for International Climate and Environmental Research-Oslo, Oslo, Norway

⁷ The Earth Institute, Center for Climate Systems Research, Columbia University, New York, USA

⁸ NASA Goddard Institute for Space Studies, New York, USA

⁹ Max Planck Institute for Chemistry, 55128 Mainz, Germany

¹⁰ Universities Space Research Association, GESTAR, Columbia, MD, USA

¹¹ School of Computer, Mathematical and Natural Sciences, Morgan State University, Baltimore, MD, USA

¹² Center for Climate System Research, University of Tokyo, Tokyo, Japan.

Abstract

An assessment of global **particulate** nitrate and ammonium aerosol based on simulations from nine models participating in the AeroCom Phase III study is presented. A budget analyses was conducted to understand the typical magnitude, distribution, and diversity of the aerosols and their precursors among the models. To gain confidence on model performance, the model results were evaluated with various observations globally, including ground station measurements over North America, Europe, and East Asia for tracer concentrations and dry and wet depositions, as well as with aircraft measurements in the Northern Hemisphere mid-high latitudes for tracer vertical distributions. Given the unique chemical and physical features of the nitrate occurrence, we further investigated the similarity and differentiation among the models by examining: 1) the pH-dependent NH_3 wet deposition; 2) the nitrate formation via heterogeneous chemistry on the surface of dust and sea-salt particles; and 3) the nitrate coarse mode fraction (i.e., coarse/total). It is found that HNO_3 , which is simulated explicitly based on full O_3 - HO_x - NO_x -aerosol chemistry by all models, differs by up to a factor of 9 among the models in its global tropospheric burden. This partially contributes to a large difference in NO_3^- , whose atmospheric burden differs by up to a factor of 13. **The atmospheric burdens of NH_3 and NH_4^+ differ by 17 and 4, respectively.** Analyses at the process level show that the large diversity in atmospheric burdens of NO_3^- , NH_3 , and NH_4^+ is also related to deposition processes. Wet deposition seems to be the dominant process in determining the diversity in NH_3 and NH_4^+ lifetimes. It is critical to correctly account for contributions of heterogeneous chemical production of nitrate on dust and sea-salt, because this process overwhelmingly controls atmospheric nitrate production (typically >80%) and determines the coarse and fine mode distribution of nitrate aerosol.

Formatted: Subscript

1. Introduction

Atmospheric aerosols adversely affect human health and play an important role in changing the Earth's climate. A series of multimodel studies have been coordinated by

50 the international activity of Aerosol Comparisons between Observations and Models
51 (AeroCom) in its Phase I and II model experiments that have systematically assessed the
52 presence and influence of almost all major atmospheric anthropogenic and natural
53 aerosols (such as sulfate, dust, and carbonaceous aerosols) (e.g., Kinne et al., 2006;
54 Schulz et al., 2006; Textor et al., 2006; Koch et al., 2009; Huneus et al., 2011; Tsigaridis
55 et al., 2014; Kim et al., 2015). Very little attention has been drawn to nitrate aerosol
56 | (hereafter “nitrate” referring to particulate nitrate unless otherwise specified) other than
57 its contribution to radiative forcing (Myhre et al., 2013). One obvious reason is that not
58 many models used to include nitrate owing to the chemical complexity of nitrate
59 formation. However, atmospheric nitrate aerosol not only exerts direct effects on air
60 quality and climate, but also uniquely impacts the Earth system by being directly
61 involved in tropospheric chemistry and constraining net primary productivity, hence
62 altering carbon sequestration and ecological effects, via its deposition (Prentice et al.,
63 2001).

64
65 Atmospheric nitrate contributes notably to total aerosol mass in the present-day,
66 especially in urban areas and agriculture regions. Nitrate is about a quarter of sulfate in
67 terms of overall global burden, AOD, and direct forcing at the present-day according to
68 the study of AeroCom II direct forcing experiment (Myhre et al., 2013). This conclusion
69 is confirmed by recent publications using various individual models and emission
70 inventories (Bellouin et al; 2011; Bauer et al., 2007; Hauglustaine 2014; Karydis et al.,
71 2016; Mezuman et al., 2016; Paulot et al., 2016). Regionally, considerable evidences
72 from in-situ measurements (Bessagnet et al., 2014; Haywood et al., 2008; Jimenez et al.,
73 2009; Malm et al., 1994; Vieno et al., 2016) and model results (Karydis et al., 2011;
74 Ensberg et al., 2013; Trump et al., 2015) indicate that nitrate becomes one of the major
75 aerosol species in urban and agriculture environments. For example, nitrate concentration
76 is about half of sulfate during the summer season in Beijing (Zhou et al., 2016) and
77 represents a large portion of wintertime aerosol mass in the San Joaquin Valley in
78 California (Pusede et al., 2016).

79
80 More importantly, the importance of aerosol nitrate is likely to increase over the century
81 with a projected decline in SO₂ and NO_x emissions and increase in NH₃ emissions (IPCC,
82 2013). With the reduction of SO₂ emissions, less atmospheric NH₃ is required to
83 neutralize the strong acid H₂SO₄. The excess of NH₃ results in gaseous HNO₃ and NH₃
84 entering the condensed phase, and their subsequent dissociation yields nitrate and
85 ammonium ions. The trend of future nitrate depends on which is the limited species, NO_x
86 or NH₃, for nitrate formation (Tsimpidi et al., 2007; 2008). Generally, our atmosphere, at
87 its current and foreseeable near future, is still in an NH₃-limited condition according to
88 sensitivity studies by Heald et al. (2012) and Walker et al. (2012). Almost all global
89 models predicted an overall increase of atmospheric nitrate burden during this century
90 based on current available emission inventories (Bauer et al 2007; 2016; Bellouin et al.,
91 2011; Hauglustaine et al., 2014; Li et al., 2014). For example, using CMIP5 future
92 emission projections, Bellouin et al. (2011) concluded that, by 2090, nitrate would
93 become an important aerosol species in Europe and Asia, contributing up to two thirds of
94 the globally averaged anthropogenic optical depth. However, the predicted trend of
95 surface nitrate is mixed. Some studies estimated a consistent increase of surface nitrate

96 (Bellouin et al., 2011), while others pointed out that this increase might vanish or even
97 reverse over some regional urban areas due to the decline of NO_x emissions (Bauer et al.,
98 2016; Pusede et al., 2016; Trail et al., 2014). Nevertheless, the potentially increasing
99 importance of nitrate in climate and its large uncertainty in future surface nitrate
100 predictions urge us to characterize model performance and understand the
101 physicochemical mechanisms behind the diversity of nitrate simulations.
102

103 Nitrate is also important in that its formation directly affects tropospheric chemistry.
104 First, the formation of nitrate, through either aqueous phase chemical reaction between
105 HNO₃ and NH₃ (Metzger et al., 2002; Kim et al., 1993) or heterogeneous reaction of
106 nitrogen species such as HNO₃, NO₃, and N₂O₅ on the surface of dust and sea salt aerosol
107 particles (Bauer et al., 2004; 2005; Bian et al., 2003; Dentener 1996; Liao et al., 2003),
108 converts gas phase nitrogen species into aerosols. Consequently, the global tropospheric
109 NO_x concentration and the rate of conversion of N₂O₅ to HNO₃ will be reduced (Riemer
110 et al., 2003), which in turn leads to the reduction of atmospheric oxidants. For example,
111 global tropospheric O₃ can be reduced by 5% (Bauer et al., 2007) and tropical Atlantic
112 OH by 10% (Bian et al., 2003) just through the heterogeneous reactions of nitrogen
113 radicals on dust. Second, the most important removal path for nitrogen from the
114 atmosphere is the formation of HNO₃, which is subsequently deposited (Riemer et al.,
115 2003). Since HNO₃ is subject to partitioning between the gas and aerosol phases, the
116 lifetimes of nitrogen species can be shortened by the formation of tropospheric nitrate
117 aerosol because the loss of total HNO₃ will be accelerated by a much higher dry
118 deposition in the aerosol phase.
119

120 Large nitrogen deposition occurs over both land and ocean (Dentener et al., 2006;
121 Kanakidou et al., 2012; 2016). Nitrogen deposition can either benefit or impair ecosystem
122 productivity depending on the initial balance of nutrients since different ecosystems have
123 different Nr (reactive nitrogen) availability and retention (Galloway et al., 2004; Prentice
124 et al., 2001). If fixed Nr is deposited as nitrate in forests, it may act as a "fertilizer,"
125 stimulating growth and thus enhancing carbon sequestration (Fowler et al., 2015). But
126 when the accumulated deposition exceeds the nutritional needs of the ecosystem, nitrogen
127 saturation may result (Fenn et al., 1996). Soil fertility declines due to the leeching of
128 cations (Milegroet and Cole, 1984) and, thus, carbon uptake diminishes. The balance
129 between fertilization and saturation depends on the spatial and temporal extent of
130 nitrogen deposition. In order to determine the extent to which the emissions of air
131 pollutants will have to be reduced and whether the environment needs to be protected
132 from damage, it is essential to know where and by how much N deposition exceeds
133 nature's tolerance (Dentener et al. 2006; Lamarque et al., 2005; Phoenix et al., 2006).
134

135 Here we present a nitrate-focused study that has been organized as a part of the series of
136 AeroCom phase III experiments (<https://wiki.met.no/aerocom/phase3-experiments>). The
137 goals of this activity are to (1) address the diversity of the nitrate simulation by the
138 AeroCom multi-models and diagnose the driving processes for the diversity, (2) explore
139 the uncertainty of the model nitrate simulations constrained against various
140 measurements from ground station networks and aircraft campaigns, and (3) investigate
141 how the formation of nitrate changes in different models in response to perturbation on

142 key precursors and factors that determine nitrate formation. We focus on the first two
143 objectives in this paper. Such a study directs us on how to improve the representation of
144 nitrate aerosol formation and size distribution in climate chemistry models and reveals
145 nitrate effects on global air quality and climate.

146
147 Building upon the analysis of the multi-model diversity, three additional sensitivity
148 experiments are designed using the GMI model to further explore the potential sources
149 for the diversity on physical and chemical process-level. First, we explore the impact of
150 pH-dependent NH_3 wet deposition on atmospheric NH_3 and associated nitrogen species.
151 We then reveal the importance of mineral dust and sea salt in the nitrate formation and
152 check the resultant nitrate aerosol size distribution that is particularly important in nitrate
153 forcing estimation.

154
155 The paper is organized as follows. Section 2 introduces the experiment setup including
156 the ~~used~~ emission inventories used and the participating AeroCom models. Observations
157 of surface tracer concentrations and dry and wet depositions over U.S., Europe, and East
158 Asia, as well as aircraft measurements in the ARCTAS campaigns are described in
159 section 3. We present AeroCom model inter-comparison and the model evaluation using
160 aforementioned observations in section 4. Based on the knowledge from previous
161 sections, we further discuss nitrate formation in response to physiochemical
162 methodologies in section 5 and summarize our major findings in section 6.

163 164 **2. Experiment setup and AeroCom model description**

165 166 **2.1 Experiment setup**

167 The AeroCom III nitrate experiment comprises one baseline and six perturbation
168 simulations, with the latter designed for assessing the possible future changes of emission
169 and meteorological fields relevant to nitrate formation. Models are advised to use the
170 same prescribed emission datasets for gases and aerosols. Emissions from anthropogenic,
171 aircraft, and ship for aerosol and ozone simulations are obtained from the recently
172 developed HTAP v2 database (Janssens-Maenhout et al., 2015) that provides high spatial
173 resolution monthly emission. For the tracers that are included in ozone chemistry but are
174 not provided by HTAP v2 (i.e. some volatile organic compounds), they should be
175 obtained from CMIP5 RCP85 with a linear interpolation between 2005 and 2010.
176 Biomass burning emissions are the emissions of GFED3 (Werf et al., 2010) in 2008
177 [<http://www.globalfiredata.org/data.html>]. The NH_3 emission from ocean is adopted
178 based on the compilation of GEIA emission inventory [Bouwman et al., 1997].
179 Participating modeling groups use their own emissions of dimethyl sulfide (DMS), dust,
180 sea salt, and NO from lightning, since they are calculated based on models'
181 meteorological fields.

182
183 A full year simulation for 2008 is required for the nitrate model experiment. There are
184 several in-situ observation datasets available in 2008 for model evaluation, including the
185 surface concentration and deposition measurements over the US (CastNet, AMoN,
186 NDAP/NTN), Europe (EMEP), and Asia (EANET), and the aircraft measurements of
187 vertical profiles (e.g. ARCTAS-A, ARCTAS-CARB, and ARCTAS-B). All participating

188 models are required to use the reanalysis or nudged meteorological data for 2008 and
189 allow ~~several months~~one-year spin up for the baseline simulation.

190

191 **2.2 AeroCom models**

192 Nine models participate in the AeroCom III nitrate experiment. Their general nitrate-
193 related physiochemical mechanisms are summarized in Table 1. Further detailed
194 information on their thermodynamic equilibrium model (TEQM) is given in Table 2.

195

196 The models participating in this study are divided into two groups. Group one (CHASER,
197 EMAC, INCA, GISS-MATRIX, and GISS-OMA) run chemical fields together with
198 meteorological fields, while group two (EMEP, GMI, OsloCTM2, and OsloCTM3)
199 simulate chemical fields using archived meteorological fields. Most models in this study
200 have a horizontal resolution around 2-3 degrees except EMEP with 0.5 degree.

201 Vertically, most models cover both the troposphere and the stratosphere with a peak
202 altitude up to 0.01 hPa except EMEP that extends vertically up to 100 hPa into the
203 troposphere only.

204

205 All models use full gas phase O_3 - NO_x - HO_x chemistry to produce HNO_3 and consider the
206 feedback of nitrate aerosol formation on HNO_3 calculation. However, due to the
207 complexity of chemical mechanisms for organic nitrate compounds and different
208 recommendations for reaction rates, HNO_3 fields produced by the models differ greatly.
209 This difference propagates into the subsequent gas-aerosol reactions for nitrate formation.

210

211 These models are very different in their approaches on gas-aerosol reactions in nitrate
212 formation. All models consider reactions between NH_3 and HNO_3 . However, models
213 differ dramatically in whether to include heterogeneous reactions on dust and sea salt
214 (Table 1). Some account for both, some for only dust or sea salt, and some do not account
215 for any of them at all. The methods used by the models in accounting for NH_3 and
216 dust/sea salt contributions are also different. Please also note that the heterogeneous
217 chemical production of nitrate mentioned in this paper refers only the reaction of HNO_3
218 on dust and sea salt particles. A series of reactions, such as N_2O_5 hydrolysis and $BrONO_2$
219 hydrolysis, affect HNO_3 simulation. These reactions are typically considered in O_3 - NO_x -
220 HO_x chemistry and their discussion is beyond the scope of this paper.

221

222 All participating models adopt TEQM to deal with aqueous and solid phase reactions and
223 gas-aerosol partitioning (Tables 1 and 2). This is based on the assumption that volatile
224 species in the gas and aerosol phases are generally in chemical equilibrium. However, the
225 assumption is not always warranted in some cases, as we will discuss in section 5.2. Even
226 with the TEQM approach, nitrate calculation could differ due to treatments of
227 equilibrium constants or chemical potentials, solute activity coefficients, water activity,
228 and relative humidity of deliquescence (RHD). The parameterizations adopted by the
229 models to deal with multicomponent activity coefficient, binary activity coefficient, and
230 water activity are given in table 2. GISS-OMA, Oslo-CTM2 and Oslo-CTM3 are special
231 in that they assume aerosols to be metastable so that the model does not take into account
232 formation of solids in this study. All other models do consider the effect of the hysteresis

233 of particle phase transitions. All models also assume that the overall particles are large
234 enough to neglect the Kelvin effect.
235
236 The participating models call the TEQMs in different ways to account for aerosol size
237 effect. All the TEQMs (ISORROPIA-I, ISORROPIA-II, MARS, RPMIRES, INCA, and
238 EQSAM3) assume particles to be internally mixed, i.e. all particles of the same size have
239 the same composition. However, some parent models (CHASER, EMEP, GMI, INCA,
240 GISS-MATRIX and GISS-OMA) call their TEQMs only once for fine mode aerosol
241 particles, while the others (EMAC, OsloCTM2 and OsloCTM3) call their TEQMs from
242 different aerosol size bins. For example, Oslo-CTM2 and Oslo-CTM3 consider a bi-
243 modal aerosol size-spectrum with two major aerosol modes, fine and coarse, and
244 calculate gas-aerosol equilibrium partitioning with EQSAM3 first for fine mode and then
245 for coarse mode. Additionally, to account for kinetic limitations, EMAC calculates the
246 phase partitioning in two stages. In the first stage, the amount of the gas-phase species
247 that is able to kinetically condense onto the aerosol phase within the model time step is
248 calculated, while in the second stage, the TEQM redistributes the mass between the two
249 phases assuming instant equilibrium (Pringle et al., 2010).
250
251 The TEQMs also differ in the chemical components considered. Specifically, the TEQMs
252 in CHASE, EMEP, GISS-MATRIX, GISS-OMA, GMI and INCA include only species
253 of sulfate, nitrate, ammonium and their gas, liquid, and solid components. The models
254 Oslo-CTM2 and Oslo-CTM3 add NaCl and HCl, while the model EMAC further expands
255 the species by including dust-related crustal material such as Ca^{2+} , K^+ , and Mg^{2+} .
256
257 These TEQMs differ in their computational approaches as well. Computational efficiency
258 is a prime consideration for a TEQM that is designed for incorporation into a global air
259 quality and climate study. To speed up the calculation, TEQMs typically divide the
260 system into sub-domains based on RH and concentrations of ammonium, sodium, crustal
261 cations, and sulfate. Corresponding approximation could be adopted for each sub-domain
262 with the minimum numbers of equilibriums and unknown components. As listed in table
263 | 2, the numbers of sub-domains are 4, 5, 4, 2, 3, and 3 for the TEQM ISORROPIA-I,
264 ISORROPIA-II, MARS, RPMIRES, INCA, and EQSAM3, respectively.
265
266 The ways to account for the contribution of dust and sea salt to nitrate formation are also
267 different. Some models (EMAC, Oslo-CTM3, and Oslo-CTM2) include dust and/or sea
268 salt components in their TEQM models directly, while some models (EMEP, GISS-
269 OMA, GMI, and INCA) use an approach of first order loss rate outside their TEQMs to
270 account for the heterogeneous reactions of HNO_3 on the surface of dust and sea salt. For
271 the latter approach, the gamma rates and their RH dependence adopted by the models
272 differ as well.
273
274 Dry and wet deposition of NH_3 , ammonium nitrate, and ammonium sulfate are treated
275 similarly to other gas and aerosol tracers in the models. It is worth pointing out that there
276 is a different consideration for Henry's law constant of NH_3 used by the models. Some
277 models modify it based on the pH value of cloud water while others do not. We will
278 discuss the impact of these two treatments on nitrate simulation in section 5.1.

279

280 We introduce only the major characteristics of thermodynamic equilibrium models since
281 this study aims for the evaluation and explanation of overall nitrate diversity among the
282 GCM/CTM models from all potential aspects. The detailed discussion of the models
283 chemical mechanism of gas phase reactions and the aerosol optical properties adopted by
284 the models is also beyond this work. Readers could refer to the references listed in Tables
285 1 and 2 for any further details.

286

287 **3. Observations**

288 We use surface measurements from ground station networks and aircraft campaigns to
289 evaluate modeled surface concentrations, dry and wet depositions, and vertical
290 distributions of nitrate and related species (Table 3).

291

292 **3.1 Surface measurements of concentrations and deposition rates**

293 Ambient concentrations of sulfur and nitrogen species throughout the US and Canada
294 have been measured by the ground station network CASTNET (Clean Air Status and
295 Trends Network) (Figure 1). The measurements use a 3-stage filter pack with a controlled
296 flow rate. The measurements of CASTNET do not include NH_3 . AMoN (Ammonia
297 Monitoring Network), measuring concentrations of ambient NH_3 , has been deployed at
298 CASTNET sites starting from October 2007 using passive samplers. The corresponding
299 tracers' surface concentration measurements over Europe have been conducted by EMEP
300 (The European Monitoring and Evaluation Programme). The measured sites of all these
301 networks are located in rural areas or sensitive ecosystems, representing a larger region
302 by avoiding influences and contamination from local sources. Surface concentrations
303 over East Asia are inferred from the measurement of dry deposition by EANET (Acid
304 Deposition Monitoring Network in East Asia). This network provides acid deposition
305 from a regional monitoring network including 13 countries in East Asia using
306 standardized monitoring methods and analytical techniques.

307

308 CASTNET also provides dry deposition of sulfate and nitrogen species. Direct
309 measurements of dry deposition fluxes (D) are expensive so D is calculated as the
310 measured pollutant concentration (C) multiplied by the modeled dry deposition velocity
311 (V_d). V_d is either estimated by the Multi-Layer Model fed with measured hourly
312 meteorological data or derived from historical average V_d for sites with discontinued
313 meteorological parameters.

314

315 Direct measurements of wet deposition fluxes of sulfate, nitrate, and other ions have also
316 been performed by NADP/NTN (the National Atmospheric Deposition Program /
317 National Trends Network) across the contiguous US, Canada, Alaska, and the US Virgin
318 Islands and EANET over East Asia. Sites are predominantly located away from urban
319 areas and point sources of pollution. Each site has a precipitation chemistry collector and
320 gauge. Both networks can measure wet deposition for a continuous period (weekly for
321 NADP/NTN and daily for EANET), or every precipitation event if using an automated
322 collector (wet-only sampling).

323

324 Data is quality assured for all measurements. Measurements over North America use
325 automated screening techniques, semi-annual calibration results, site operator comments,
326 and manual data review. Quality assurance of EMEP is carried out on both the national
327 level and by the Chemical Co-ordinating Centre (CCC). The quality of EMEP
328 measurements is not equal at the national level (Schaap et al., 2002; 2004). Sites in
329 North, Western and Central Europe were generally well equipped and performing, while
330 sites in the rest of Europe suffered from inadequate sampling and calibrating methods due
331 to political and/or economical reasons. The quality of ammonia measurement is relatively
332 low since some laboratories experienced contamination problems (Williams et al., 1992).
333 Although EANET adopts standardized monitoring methods and analytical techniques,
334 quality assurance is carried out on the national level.

335

336 **3.2 Aircraft measurements of vertical profiles**

337 Aircraft campaign measurements during the 2008 Arctic Research of the Composition of
338 the Troposphere from Aircraft and Satellites (ARCTAS) are used to evaluate tracer
339 vertical distribution simulated by the models (Bian et al., 2013; Jacob et al., 2010). Three
340 phases of the campaign, ranging from Northern Hemisphere mid-latitude industrial
341 region (ARCTAS-CARB, June 2008) to high latitude Arctic regions influenced by long-
342 range pollution transport (ARCTAS-A, April 2008) and by local boreal biomass burning
343 (ARCTAS-B, July 2008), provide well encompassing environment observations. All
344 flights were conducted by the NASA DC-8 aircraft and the flight tracks of these three
345 phases are presented in Figure 2. An onboard HR-ToF-AMS instrument (Cubison et al.,
346 2011; DeCarlo et al, 2006) measured fine mode aerosol concentrations (PM₁) along the
347 flight track including NO₃⁻, NH₄⁺, and SO₄²⁻ at STP conditions (1013mb and 273.15K) at a
348 sampling time interval of ~12 seconds. Accuracy estimate of 2-standard deviations, likely
349 conservative, is 34% for inorganics, dominated by the uncertainty in particle collection
350 efficiency due to particle bouncing (Huffman et al., 2005).

351

352 **4. Model intercomparison and evaluation**

353

354 **4.1 AeroCom model inter-comparisons of global distributions and budgets**

355 **4.1.1 NH₃ and NH₄⁺**

356 Six models use HTAP2 anthropogenic emissions, two (GISS-MATRIX and GISS-OMA)
357 use CMIP5 emissions, and one (INCA) uses ECLIPSE emissions. Table 4b shows that
358 eight models have the annual NH₃ emission values within 5% of the value from the
359 AeroCom experiment recommended emission inventories, but INCA is 11% higher. The
360 similar emission distributions ensure that the examined inter-model diversities are truly
361 caused by the differences in physicochemical processes among the models. The
362 normalized root-mean-square deviation (NRMSD) of NH₃ global burden among models
363 is 1.17 and 0.33 with and without EMAC included. This drastic change in global burden
364 NRMSD by EMAC is caused by its special treatment of wet deposition. In fact, the
365 removal of trace gases and aerosol particles by clouds and precipitation in EMAC is not
366 calculated based on empirically determined, fixed scavenging coefficients, but rather by
367 solving a system of coupled ordinary differential equations, explicitly describing the
368 processes involved (Tost et al., 2006). This method resolves feedback mechanisms
369 between the multi-phase chemistry and transport processes involved. The liquid phase

370 reaction set used converts all the scavenged NH_3 (or HNO_3) into NH_4^+ (or NO_3^-) in the
371 liquid phase so that at the end everything that is deposited is the total NH_4^+ and NH_3 .
372

373 Atmospheric NH_4^+ is produced entirely by NH_3 chemical transformation. The models
374 simulate NH_4^+ much closer in chemical production (difference less than a factor of 2) than
375 in lifetime (difference up to a factor of 5.2), indicating removing rates are a key factor in
376 controlling the global burden of NH_4^+ . For example, CHASER has a much longer lifetime
377 of NH_4^+ (i.e. 9.8 days versus 4.3 days in average), which indicates a slow deposition
378 removal of NH_4^+ from the atmosphere. Consequently, CHASER simulates a much higher
379 atmospheric NH_4^+ burden than other models.

380 381 **4.1.2 HNO_3 and NO_3^-**

382 HNO_3 , an important nitrate precursor, differs by up to a factor of 9 in its global
383 tropospheric burden among the models (Table 4c). All models simulated HNO_3 based on
384 a full gas phase O_3 - HO_x - NO_x chemistry and coupled it with aerosol chemistry. This
385 HNO_3 diversity will naturally be propagated into the NO_3^- simulation. However, further
386 discussion of the detailed consideration of full gas-aerosol chemistry for HNO_3 diversity
387 among the models is beyond the scope of this study.
388

389 The resultant aerosol product (i.e., NO_3^-) does not entirely follow its precursor (i.e.,
390 HNO_3) in terms of global burden: EMEP has very low HNO_3 but high NO_3^- , two GISS
391 models (MATRIX and OMA) simulate high HNO_3 but low NO_3^- , while OsloCTM3 has
392 an average HNO_3 but more than triple high NO_3^- than average (Tables 4a and 4c).
393 Furthermore, the difference in NO_3^- global burden (up to a factor of 13) is larger than that
394 of HNO_3 . Differences in chemical mechanisms of NO_3^- production could be a potential
395 explanation along with the difference in HNO_3 precursor. Unfortunately, only GMI and
396 INCA provide a detailed NO_3^- chemistry budget analysis. Nevertheless, we can infer that
397 the total chemical production of NO_3^- must be very low ($\sim 10\text{Tg}$) in the two GISS models
398 while very high ($> 100\text{Tg}$) in OsloCTM2 and OsloCTM3 based on the reported total
399 NO_3^- loss. Combining this information with the HNO_3 global tropospheric burden (Table
400 4c), we can further infer that the chemical conversion from HNO_3 to NO_3^- must be lowest
401 in the two GISS models while highest in the two Oslo models. Several factors could
402 influence this conversion, such as the availability of alkaline species of mineral dust and
403 sea-salt particles and the physicochemical mechanism of nitrate formation on dust and
404 sea-salt, availability of NH_3 after combining with SO_4^{2-} , and the atmospheric
405 meteorological fields of temperature and relative humidity. More discussions are given in
406 sections 5.2 and 5.3.
407

408 Atmospheric lifetime of NO_3^- differs up to a factor of 4, from about 2 days in GMI and
409 OsloCTM2 to larger than 7 days in GISS-OMA and GISS-MATRIX. The slower removal
410 processes in the two GISS models compensate the low chemical production and help to
411 maintain their NO_3^- atmospheric burden (Figure 3 and Table 4a).
412

413 **4.2 Model-observation comparisons**

414

Formatted: Subscript

Formatted: Subscript

Formatted: Subscript

415 **4.2.1 Comparisons of surface concentrations over North America, Europe, and East**
416 **Asia**

417 Understanding diversity among model simulations and potential physiochemical
418 processes behind the difference is important but not sufficient. The information has to be
419 combined with the knowledge of model performance obtained directly from comparisons,
420 particularly down to processes level, against various measurements to gain a direction of
421 any improvement. Figures 4a-c show a model-observation comparison for surface
422 mass/volume mixing ratios of NO_3^- , NH_4^+ , NH_3 , HNO_3 , and SO_4^{2-} over North America
423 (CastNET), Europe (EMEP), and East Asia (EANET). Each point represents a monthly
424 mean concentration at one observational site. Generally, the agreement between model
425 and observation is better for aerosol components than for gas tracers (i.e. the precursor
426 species NH_3 and HNO_3) over all three regions. All models underestimate NH_3 surface
427 volume mixing ratio with a ratio of model to observation down to 0.14, while most
428 models overestimate surface HNO_3 volume mixing ratio with a ratio up to 3.9 over North
429 America. The worse performances of NH_3 against observations may be also associated to
430 their relatively lower measurement accuracy, i.e. easier to be contaminated during
431 measurement (Williams et al., 1992). Among aerosol simulations, model performance is
432 very similar for NH_4^+ and SO_4^{2-} , while slightly worse for NO_3^- that is dispersed further
433 away from the 1:1 line, particularly at low NO_3^- values. The NO_3^- simulation over East
434 Asia is worst with the average normalized root mean square to be 1.3 and 1.8 higher than
435 that over North America and Europe, respectively.

436
437 **4.2.2 Comparisons of vertical profiles with aircraft measurements during the**
438 **ARCTAS field campaign**

439 Evaluation of model performance presented in 4.2.1 for the surface concentrations in the
440 source regions is highly dependent on the accuracy of the emission inventory. On the
441 other hand, evaluation using aircraft measurements, particularly over remote regions,
442 provides further examination of models' physicochemical evolution during transport.
443 Here we use data from three phases of the ARCTAS aircraft campaign (section 3), and
444 the results are shown in Figure 5. All model results of NO_3^- , NH_4^+ , and SO_4^{2-} are sampled
445 along flight track and averaged regionally within 1km vertically for each campaign phase
446 before comparing with the corresponding aircraft measurements. Note that only EMAC,
447 EMEP and GMI report daily 3D global tracer concentrations, while the others report
448 monthly only. Note also that only EMEP and GMI adopt daily biomass burning emission
449 while the others use monthly emission. To verify the representativeness of monthly mean
450 concentration in capturing the main features exhibited in model-observation comparisons,
451 daily and monthly concentrations of the three models are used in the same spatial
452 sampling to compare with the measurements (see the green lines for daily and red for
453 monthly in the figure). The comparison keeps its main features as shown when using both
454 daily and monthly model data.

455
456 During ARCTAS-A, which was conducted in April 2008 and was based in Fairbanks,
457 Alaska, none of the models captures the long-range transport of aerosols primarily from
458 Asia, which enter Polar Regions at altitudes between 2-7 km (Fig. 3 in Bian et al., 2013).
459 Except CHASER and EMAC, all models also report a significant underestimation of
460 NH_4^+ and SO_4^{2-} in boundary layer. A previous assessment of pollution transport to the

461 Arctic indicated that aerosol wet removal plays an important role in the uncertainty of
462 Arctic aerosols (Shindell et al., 2008). Another potential reason is that some large fire
463 activities in Siberia during April 2008 (Jacob et al., 2010) may be missed in the GFED3
464 emission inventory. The underestimation of SO_4^{2-} may help bring up NO_3^- production,
465 particularly at high altitudes. During ARCTAS-CARB, which was conducted in June
466 2008 based in Palmdale, California, agreement between model and measurements is
467 much improved. Almost all models show a rapid vertical decrease from surface to free
468 troposphere, which is consistent with the measurements of SO_4^{2-} and NH_4^+ , but not NO_3^- .
469 The observation shows a maximum of NO_3^- at about 1.5 km, which is not represented by
470 any of the models. During ARCTAS-B, which was conducted in July 2008 and was based
471 in Cold Lake, Canada, when there were frequent local wild fires, model performances are
472 mixed. In general, most models underestimate concentrations of NO_3^- , NH_4^+ and
473 SO_4^{2-} below 4 km. CHASER model is special in that it overestimates SO_4^{2-} significantly.
474 This may be contributed to high (near surface) to comparable (free troposphere) model
475 simulation of NH_4^+ but an underestimation of NO_3^- . Different from other models, the
476 INCA model shows an enhancement of pollutants in the upper troposphere with
477 concentrations much higher (more than 5 times) than observations. This behavior may be
478 derived from a much vigorous vertical uplifting to the upper troposphere as revealed from
479 Fig. 3a-3b combined with a low NH_3 Henry's law constant used by INCA, see discussion
480 in section 5.2.

481
482 Note that all measurements and model data we discussed above are for fine mode
483 aerosols. Total NO_3^- (orange line using monthly model output) is also shown in the figure
484 to reveal whether a changing of partitioning of fine and coarse mode NO_3^- could improve
485 the model-observation comparison. It seems that the new version of OsloCTM3 may put
486 too much of NO_3^- in coarse mode.

488 **4.3 Model-observation comparison for dry and wet deposition**

490 **4.3.1 Dry deposition**

491 The budget analyses in section 4.1 concluded that dry and/or wet depositions are most
492 likely the main processes driving the diversity in the model simulations. Thus, further
493 evaluation of deposition processes is needed to identify any potential problematic model.

494
495 The dry depositions of NO_3^- , NH_4^+ , HNO_3 , and SO_4^{2-} simulated by the models are
496 compared against CASTNET measurements over North America (Figure 6). Generally,
497 the overestimation of surface HNO_3 concentrations (Figure 3a) results in the higher dry
498 depositions of HNO_3 , but this is not the case for NO_3^- . Meanwhile, most of the models
499 give a better dry deposition simulation for aerosol SO_4^{2-} and NH_4^+ than for aerosol NO_3^- ,
500 except CHASER. Specifically, GISS-OMA and GISS-MATRIX have wide spread dry
501 NO_3^- deposition at any given measurement value. In other words, the two models
502 underestimate NO_3^- dry deposition significantly at many observational stations, which
503 does not occur in the other models. This low dry deposition simulation may occur outside
504 North America as well because the global dry depositions of the two models are lower
505 than others (Table 4a). OsloCTM2 overestimates NO_3^- dry deposition significantly, which
506 is probably linked to its larger coarse fraction of the nitrate aerosol (see discussion in

507 section 5.3). OsloCTM3 improved its dry deposition scheme although the model still
508 overestimates the dry deposition. We will discuss the OsloCTM2 NO_3^- simulation over
509 North America by combining the model's wet deposition in the next section. NH_4^+ dry
510 deposition is low in GMI but very high in CHASER. This performance is also extended
511 globally as summarized in Table 4b.

512

513 4.3.2 Wet deposition

514 The wet deposition simulations from the nine models are compared with surface
515 measurement over North America (Figure 7a) and East Asia (Figure 7b) for oxidized
516 NO_3^- (i.e. total NO_3^- and HNO_3), total NH_4^+ and NH_3 (tNH_4^+), and SO_4^{2-} . All models tend
517 to underestimate the wet deposition of tNH_4^+ and SO_4^{2-} over the two regions. Models
518 EMAC, GMI, OsloCTM2 and OsloCTM3 have relatively high wet removal for oxidized
519 NO_3^- , while EMEP removes much less than others over North America. All models' wet
520 deposition of oxidized NO_3^- is biased low over East Asia. As we discussed above,
521 OsloCTM2 and OsloCTM3 have very high dry NO_3^- depositions (Figure 6) compared
522 with CASTNET observations. The overall high dry and wet NO_3^- depositions along with
523 high atmospheric concentrations (Figure 4a) indicate that the chemical formation of
524 NO_3^- in the two models must be also high. This performance might be also true on global
525 scale since the inferred chemical productions of NO_3^- in the two models are the highest
526 (Table 4a). CHASER has the lowest tNH_4^+ wet deposition. This may result in a very high
527 NH_4^+ dry deposition (Figure 6) and concentration (Figures 4a-c, 5) compared with
528 observations and other models. Overall, wet deposition seems to be the dominant process
529 in determining the diversity in NH_3 and NH_4^+ lifetime (Table 4b).

530

531 Note that we use the traditional approach of comparing models' grid box mean values
532 with observations, which does not take into account the impact of the models' horizontal
533 resolutions in their representation of observations (Schutgens et al., 2016). Since majority
534 models (except EMEP) have horizontal resolutions around 2-3 degrees, the models grid
535 box means tend to smooth out extreme (i.e. very low or high) observations. Reflecting on
536 the scattering plots of model (y axis) and observation (x axis) is that the slopes of fitting
537 lines are generally less than 1 (Figures 4a-d, 6, 7a-b). Consequently, the slopes of the
538 fitting lines are generally less than 1 on the scattering plots with model as y-axis and
539 observation as x-axis (e.g. Figures 4a-d, 6, 7a-b).

540

541 5. Discussion of major uncertainties in nitrate formation

542 Large uncertainties of nitrate studies result from the complexity of the simulations which
543 must consider a comprehensive NO_x -NMHC- O_3 - NH_3 chemistry and a thermodynamic
544 equilibrium model (TEQM) to partition semi-volatile ammonium nitrate between the gas
545 and aerosol phases. Nitrate aerosol concentrations depend on temperature, relative
546 humidity (RH), and concentrations of HNO_3 , NH_3 , NH_4^+ , SO_4^{2-} , Cl^- , Na^+ , Ca^{2+} , K^+ ,
547 Mg^{2+} , organic acids, among others. A further complicating factor is that the equilibrium
548 for the coarse mode is somewhat questionable (Feng and Penner, 2007). In addition, wet
549 removal of NH_3 is very sensitive to the ~~correction of~~ pH in cloud water. We will discuss
550 some of these uncertainties below.

551

552 5.1 pH-dependent NH_3 wet deposition

Formatted: Highlight

553 Gas tracer NH₃, a precursor of ammonium aerosol, experiences atmospheric wet
 554 deposition and its deposition rate is typically calculated using Henry's Law. Henry's law
 555 constant (H) of gases in water is usually given at 298 K (indicated by Θ in superscript)
 556 and can be adjusted by temperature (T).

$$H(T) = H^{\Theta} * \exp\left(-\frac{\Delta H_{sol}}{R}\left(\frac{1}{T} - \frac{1}{T^{\Theta}}\right)\right) \quad (1)$$

557 Here ΔH_{sol} is the enthalpy of dissolution and R is the gas constant.

558

559 For some acidic/basic gases, including NH₃, Henry's law constant is also a function of
 560 pH in cloud water (a.k.a effective Henry's law constant H^{Θ*}). As explained in the
 561 Appendix, the H^{Θ*} is inferred from H^Θ with a correction of pH (pH = -log₁₀[H⁺]) as

$$H^{\Theta*} = H^{\Theta} \frac{K_{al}[H^+]}{K_w} \quad (5)$$

562 Here, K_{al} ≈ 1.8x10⁻⁵ and K_w = 1.0x10⁻¹⁴ at 298 K in pure water (see Appendix). However,
 563 not every model accounts for pH adjustment (i.e. the reaction of equation 2 in Appendix)
 564 for NH₃ dissolution. More accurately, the EMAC model implicitly calculates the
 565 effective Henry's law constant by solving a set of partial differential equations, which
 566 includes not only the gas-liquid phase equilibria, but also the reactions in the liquid phase
 567 (i.e. dissociation or acid-base equilibria, Redox reactions and photolysis reactions in the
 568 liquid phase, see Tost et al.(2006)). Therefore, the gas-liquid phase equilibrium is
 569 explicitly calculated based on the chemical mechanism used in the liquid phase. As listed
 570 in Table 5, the rest of the models are generally divided into two groups based on their
 571 effective Henry's law constant: (1) INCA, GISS-OMA and GISS-MATRIX has H^{Θ*} ≤
 572 100 (L-theta without pH correction) and (2) CHASER, GMI, OsloCTM2 and Oslo-
 573 CTM3 has H^{Θ*} > 10⁺⁵ (H-theta with pH correction). The NH₃'s H^{Θ*} adopted by the
 574 models varies dramatically, up to an order of 6 in magnitude among all the models and a
 575 factor of 10 just for the models in H-theta group (Table 5). **The latter is corresponding to**
 576 **a correction for a range of pH ranging from 4.5 (Oslo-CTM2) to 5.5 (CHASER).**

Formatted: Highlight

Formatted: Highlight

Formatted: Highlight

578 To examine how sensitive of NH₃, NH₄⁺ and NO₃⁻ simulations in response to the
 579 magnitude of NH₃'s H^{Θ*}, we performed a sensitivity experiment, named TWET, in the
 580 GMI model in which there was no pH adjustment for NH₃ Henry's law constant (i.e.
 581 H^{Θ*}=61 instead of 1.05e+6, see table 6). The resultant annual budgets of dry/wet
 582 deposition, chemistry production and loss, and atmospheric loading of NH₃,
 583 NH₄⁺ and NO₃⁻ are summarized in Table 7, the tracers' vertical zonal mean distributions
 584 are shown in Figure 8, and the comparisons with the ARCTAS measurements for
 585 NH₄⁺ and NO₃⁻ are shown in Figure 9. For convenient comparison, the GMI baseline
 586 results are given in the table and figures as well. There is a dramatic decrease (from 17.5
 587 to 1.1 Tg) in NH₃ wet deposition when using pure water NH₃ Henry's law constant.
 588 Consequently, NH₃ will remain in the atmosphere (i.e. ~ 8 times more atmospheric NH₃)
 589 to produce ~1.6 times more NH₄⁺ chemically. This, in turn, greatly increases atmospheric
 590 NO₃⁻ to 0.97 Tg from 0.26 Tg reported in baseline simulation. A large portion of the
 591 increased NH₃, NH₄⁺ and NO₃⁻ resides in the upper troposphere and close to the
 592 tropopause region, while the changes of the tracers in the lower troposphere are relatively
 593 small, as shown in Figure 8. These accumulations at high altitudes are far above (i.e. ~ 50
 594 times for NH₄⁺ and NO₃⁻) the ARCTAS observed tracer amounts as shown in Figure 9.

595 The TWET experiment might be an explanation of NH_4^+ and NO_3^- accumulations near the
596 tropopause region (Figure 3a-b) in the INCA model whose NH_3 Henry's law constant H^\ominus
597 is 74 without pH correction (i.e. a L-theta model, table 5). However, it is puzzling that the
598 NH_3 simulations by GISS-MATRIX and GISS-OMA, those are the models with L-theta,
599 are closer to the simulations of the models with H-theta, i.e. no NH_4^+ and NO_3^-
600 accumulation near the tropopause and comparable removal of NH_4^+ (Figure 3a-b and
601 Table 4b).

602

603 **5.2 Contribution of dust and sea salt on nitrate formation**

604 In the presence of acidic accumulation-mode sulfuric acid containing aerosols, HNO_3 ,
605 NO_3 radicals, and N_2O_5 will deposit on larger alkaline mineral or salt particles (Dentener
606 et al., 1996; Gard et al., 1998; Hauglustaine 2014; Karydis et al., 2016; Murphy and
607 Thomson 1997; Paulot et al., 2016). Considerable evidence shows that the majority of
608 atmospheric nitrate is formed via reactions associated with dust and sea salt (Allen et al.
609 2015; Itahashi et al., 2016; Karydis et al., 2016). Coarse mode nitrate overwhelmingly
610 dominates over remote oceanic regions (Itahashi et al., 2016). Over wide land regions,
611 nitrate also quite often exists in the form of supermicron NO_3^- balanced by the presence
612 of mineral cations arising from transport of crustal dust and sea spray aerosol (Allen et
613 al., 2015; Lefer and Talbot, 2001).

614

615 Investigation of nitrate interactions with mineral dust and sea salt depends on the
616 simulation approach adopted in a model. The traditional equilibrium approach to partition
617 semi-volatile HNO_3 between the gas and aerosol phases is no longer possible since the
618 time to reach equilibrium on coarse mode particles (several hours to days) is typically
619 much longer than the chemical time step used in a global model (less than 1 hour) (John
620 et al., 1989; Myhre et al., 2006). Meng and Seinfeld (1996) found that on longer time
621 scales, when NH_3/HNO_3 started to condense on larger aerosols, their gas phase
622 concentrations decreased so that some of the condensed matter can be driven back to the
623 gas phase from the small semi-volatile aerosols. A fix to a non-equilibrium state would
624 be to implement a kinetic formulation for the particles that have a long equilibrium time
625 scale (Feng and Penner, 2007; Karydis et al., 2010). However, implementing explicit
626 kinetics in a global model would be computationally expensive and, hence, is not feasible
627 for long-term climate simulations. Several approximations, therefore, have been
628 developed to compromise accuracy and efficiency.

629

630 Four such approximations are adopted by the nine models participating in this study: 1)
631 using equilibrium calculations for fine mode particles only while neglecting nitrate
632 formation on coarse mode particles (CHASER and GISS-MATRIX); 2) combining
633 equilibrium calculation for a solution of $\text{SO}_4^{2-}-\text{NO}_3^- - \text{NH}_4^+ - \text{H}_2\text{O}$ and heterogeneous
634 reaction calculation for nitrogen uptake on dust and sea-salt using a first-order loss rate
635 (EMEP, GMI, GISS-OMA and INCA); 3) running equilibrium model including NH_3 ,
636 dust and sea salt repeatedly for aerosol sizes from fine mode to coarse mode (Oslo-CTM2
637 and Oslo-CTM3); and 4) using only the fraction of the gas that can kinetically condense
638 within the time step of the model in the equilibrium calculations for each aerosol size
639 mode (EMAC).

640

641 Nitrate is formed primarily on dust and sea salt by GMI (88%) and INCA (82%) (see
642 Table 4a). INCA further separates the formation as 45% on dust and 37% on sea-salt. The
643 above-mentioned approach 1 is problematic due to absence of coarse mode nitrate, an
644 important portion of nitrate, which results in relatively low nitrate burdens for CHASER
645 and GISS-MATRIX. Unfortunately, the other models are missing a detailed nitrate
646 chemistry budget report. A potential impact of dust and sea-salt on nitrate formation,
647 nevertheless, can be inferred from the approach adopted by a model. For example,
648 OsloCTM2 and OsloCTM3 adopt approach 3. Although the model allows fine mode
649 particles to reach equilibrium first, the subsequent equilibrium calculation for coarse
650 mode particles may still produce coarse mode nitrate too quickly, see discussion of the
651 ratio of coarse mode nitrate in the next subsection. To avoid such overestimations on the
652 production of coarse mode nitrate, EMAC allows only a fraction of HNO_3 to partition in
653 the aerosol phase by assuming diffusion limited condensation (Pringle et al., 2010).

654

655 To further understand the role of homogeneous and heterogeneous chemical reaction
656 processes in nitrate formation, we conducted two more sensitivity experiments,
657 TnoCNH3 and TnoCHET, with the GMI model (Table 6). Experiment TnoCNH3 turned
658 off chemical conversion of NH_3 to NH_4^+ in the GMI thermodynamic equilibrium model,
659 while experiment TnoCHET excluded the nitrate formation via heterogeneous reaction of
660 gas HNO_3 on the particles of dust and sea salt. The budget report, vertical zonal mean
661 distribution and model-observation comparison of NH_3 , NH_4^+ and NO_3^- are given in Table
662 7 and Figures 8-9, respectively. It is not surprising that experiment TnoCNH3 gives a
663 higher atmospheric NH_3 burden (0.32 Tg) compared with baseline (0.11 Tg) with little
664 NH_4^+ left (from its initial field). The interesting thing is that the formed NO_3^- has only
665 slightly decreased compared with baseline (from 0.26 to 0.20 Tg), confirming the
666 importance of NO_3^- formation via dust and sea salt. For experiment TnoCHET, the
667 simulations of NH_3 and NH_4^+ stay the same but the formed NO_3^- is decreased dramatically
668 (from 0.26 to 0.10), indicating that NO_3^- formation via NH_3 chemistry alone in the GMI
669 model is relatively small. The chemical production of NO_3^- is about 6 times larger in
670 TnoCNH3 (via dust and sea salt) than in TnoCHET (via NH_3). However, the NO_3^-
671 produced via NH_3 chemistry (TnoCHET) is non-negligible over remote regions impacted
672 by long-range transport, as shown in the analysis of April Alaska observations in Figure
673 9.

674

675 **5.3 Nitrate size distribution**

676 Unlike sulfate aerosol, a noticeable fraction of nitrate aerosol is in the coarse mode.
677 Having an accurate aerosol size distribution is critical in climate forcing estimations,
678 since large size particles have a relatively small optical cross section at a given aerosol
679 mass loading and the nitrate material coating on dust particles has almost no direct impact
680 on the dust optics, although the greatly impact dust lifetime (Bauer et al., 2007). Given
681 that the deposition velocity of a coarse particle is greater than that of a fine particle, an
682 accurate size distribution is also necessary to estimate deposition of particulate nitrates
683 (Yeaman et al., 2001; Sadanaga et al., 2008). This estimation is particularly important
684 over oceans where coarse mode nitrate dominates (Itahashi et al., 2016) and nitrogen
685 supply is often in deficit (Hansell and Follows, 2008).

686

687 As we have discussed in section 5.2, nitrate size distribution varies with the approaches
688 adopted for nitrate formation on coarse mode aerosols (i.e. dust and sea salt). Figure 10
689 gives the burdens of nitrate in fine mode and coarse mode portions and the ratio between
690 coarse mode and total (f_c) for the eight discussed models. The ratio is ranging from 0
691 (CHASER and GISS-OMA), ~50% (EMAC, GMI and INCA), ~80% (EMEP and
692 OsloCTM2), and 97% (OsloCTM3). The two OsloCTMs give the highest f_c partially
693 because they run TEQM model for coarse model particles.

694

695 A wide range of f_c , from 0 to > 90%, has been reported previously by model simulations
696 (Adams et al., 2001; Bauer et al., 2007; Jacobson 2001), while the range is narrowed
697 down to 40-60% for the model studies using the approach that solves dynamic mass
698 transfer equation for coarse mode particles (Feng and Penner, 2007; Xu and Penner,
699 2012).

700

701 It is worth pointing out that aerosol microphysics modify aerosol size as well. For
702 example, a process like coagulation would also allow NO_3^- to mix with other particles and
703 enter coarse mode aerosol. New particle formation/nucleation would add $\text{NH}_3/\text{NH}_4^+/\text{NO}_3^-$
704 into the ultra fine mode. Except EMAC and GISS-MATRIX, majority models involved in
705 this study are bulk aerosol models that do not account for aerosol microphysics.

706

707 It is challenging to verify the nitrate size distribution globally due to the limited
708 measurements on time and space. Measurements over regional and station sites indicated
709 that the ratio of f_c could be very high and vary seasonally over oceanic sites. For
710 example, annual mean f_c during 2002-2004 from the Fukue supersite observatory is
711 about 72% with a seasonal variation of 60–80% in winter and of around 80% in summer
712 (Itahashi et al., 2016).

713

714 However, the ratio could be varied dramatically over land or the areas affected by land
715 pollution. For example, observations of fine and coarse particulate nitrate at several rural
716 locations in the United States indicated that nitrate was predominantly in submicron
717 ammonium nitrate particles during the Bondville and San Gorgonio (April) campaigns, in
718 coarse mode nitrate particles at Grand Canyon (May) and Great Smoky Mountains
719 (July/August), and both fine and coarse mode nitrate during the studies at Brigantine and
720 San Gorgonio (July) (Lee et al., 2008). Allen et al. (2015) examined aerosol composition
721 data collected during the summer 2013 SOAS and concluded that inorganic nitrate in the
722 southeastern United States likely exists in the form of supermicron NO_3^- , balanced by the
723 presence of mineral cations arising from the transport of crustal dust and sea spray
724 aerosol. The measurements over Harvard Forest, a rural site in central Massachusetts,
725 supported that the majority of nitrate mass was associated with water-soluble
726 supermicron soil-derived Ca^{2+} in an acidic environment (Lefer and Talbot, 2001).

727 Measurements of coarse-mode aerosol nitrate and ammonium at two polluted coastal
728 sites, Weybourne, England and Mace Head, Ireland, during polluted flow when the air
729 had passed over strong source regions of the UK and northern Europe, showed 40–60%
730 of the nitrate was found in particles with diameter >1 μm , but under clean marine
731 conditions almost 100% conversion was seen (Yeatman et al., 2001).

732

733 6. Conclusions

734

735 We present the AeroCom phase III nitrate study by assessing aerosol simulations of
736 nitrate and ammonium and their precursors with nine global models. Five of the models
737 couple the chemical calculation online with meteorological simulation, and four use
738 archived meteorological fields driving chemistry. To focus on chemical-physical
739 processes behind the diversity of nitrate simulation, all participating models are
740 encouraged to use HTAP2 emission inventory [for aerosol and gas emissions from](#)
741 [anthropogenic, aircraft, and ship sources](#). The simulated aerosols of nitrate and
742 ammonium and their precursors are compared among the models and evaluated against
743 various measurements including surface concentrations and dry/wet depositions from
744 surface measurements, and vertical distributions from aircraft measurements.

745

746 All models capture the main features of the distribution of nitrate and ammonium: large
747 surface and column amounts over China, South Asia, Europe, and U.S. These regions are
748 typically densely populated with large NH_3 and NO_x emissions. Many models also show
749 enhanced nitrate and ammonium over the Middle East and continents over the Southern
750 Hemisphere. The former undergoes huge dust pollution and the latter experiences fires
751 that emit both NH_3 and NO_x .

752

753 The diversity of nitrate and ammonium simulations among the models is large: the ratio
754 of the maximum to minimum quantities among the nine models is 13.4 and 4.4 for model
755 simulated global mass burdens of nitrate and ammonium, respectively, and 3.9 and 5.2
756 for the corresponding lifetimes. These values are also larger than those of sulfate: 4.0 for
757 global burden and 3.0 for lifetime.

758

759 The agreement between models and observations is better for aerosol components than
760 for gas tracers. All models underestimate NH_3 surface mass concentrations but most
761 models overestimate surface HNO_3 concentrations over North America and East Asia.
762 Performance of NH_3 is the worst: this could partially be associated to its relatively lower
763 measurement accuracy, i.e. a loss of ammonia possibly on the filters designed to collect
764 NH_3 (Williams et al., 1992). Among aerosol simulations, model performance based on
765 evaluation of surface mixing ratio and dry/wet depositions is very similar for NH_4^+ and
766 SO_4^{2-} , while slightly worse for NO_3^- . Models severely underestimate the aerosol
767 concentrations with only a few exceptions when compared with aircraft measurements
768 and this problem is worse over regions impacted by long-range transport than those
769 closer to sources.

770

771 There are many intrinsic reasons for a larger diversity in nitrate simulations among
772 models. Nitrate is involved in much more complicated chemistry: the chemical
773 mechanism needs to handle a multiphase multicomponent solution system. The system
774 sometimes cannot even be solved using the thermodynamic equilibrium approach when
775 coarse mode dust and sea salt particles present. A reasonable nitrate simulation also
776 depends on good simulations of various precursors, such as NH_3 , HNO_3 , dust and sea
777 salt, although models account for impact of dust and sea salt very differently. Even an
778 accurate simulation of SO_4^{2-} is a prerequisite because SO_4^{2-} surpasses NO_3^- at reacting

Formatted: No widow/orphan control, Don't adjust space between Latin and Asian text, Don't adjust space between Asian text and numbers

779 with NH_4^+ .

780

781 The models' intercomparison and model-observation comparison revealed at least two
782 critical issues in nitrate simulation that demand further exploration: NH_3 wet deposition
783 and relative contribution to NO_3^- formation via NH_3 and dust/sea salt. The nine
784 participating models adopt very different effective Henry's law constants for NH_3 , with
785 one group having a value equal or less than 100 (in pure water) and the other larger than
786 $1.e+05$ (with pH correction). Sensitivity studies using the GMI model indicated that
787 without pH correction, NH_3 wet deposition decreases massively (from 17.5 to 1.1 Tg),
788 which prolongs atmospheric NH_3 lifetime (from 0.67 to 5.2 days) and enhances its
789 atmospheric burden (from 0.11 to 0.85 Tg), and thus the atmospheric burden of NH_4^+
790 (from 0.17 to 0.48 Tg) and NO_3^- (from 0.26 to 0.97 Tg) as well. These enhanced tracers
791 tend to accumulate in the upper troposphere and close to the tropopause, and are too high
792 when compared with aircraft measurements. Since liquid-phase reaction 2 in Appendix
793 can reach equilibrium quickly within a chemical time step, we recommend including it in
794 accounting for NH_3 solution. Theoretically, a more accurate approach is to combine wet
795 removal with liquid-phase chemistry calculation. In other words, instead of using an
796 implicit calculation of effective Henry's law constant, the gas-liquid phase equilibrium is
797 explicitly calculated based on the chemical mechanism used in the liquid phase. The
798 solution of NH_3 is calculated by solving a set of partial differential equations, which
799 includes not only the gas-liquid phase equilibrium, but also all the important reactions in
800 the liquid phase, as adopted in EMAC model.

801

802 All the models use thermodynamic equilibrium to solve the chemical process of
803 $\text{NH}_3/\text{NH}_4^+$ to NO_3^- formation in fine model aerosols. However, the models adopt very
804 different ways in accounting for the contribution of these reactions on the surface of dust
805 and sea salt particles: some account for both dust and sea salt, some account for only dust
806 or only sea salt, and two models even do not account for any heterogeneous reactions.
807 The methodologies that take dust and sea salt into account are also very different, i.e.
808 together with NH_4^+ using thermodynamic equilibrium model or simply adopting a first
809 order loss rate on dust and sea salt surfaces. The chemical budget reported by GMI and
810 INCA indicates that the majority (>80%) of global NO_3^- formation is via reaction on dust
811 and sea salt. Two sensitivity experiments using the GMI model by tagging the NO_3^-
812 formation from either $\text{NH}_3/\text{NH}_4^+$ chemistry or heterogeneous reactions on dust and sea
813 salt confirm the critical importance of the latter process, and indicate that the former
814 process is relatively important in remote regions. The importance of NO_3^- formation on
815 dust and sea salt lies also in its determination on nitrate particle size distribution, so that
816 has an implication in air quality and climate studies as well.

817

818 Our work presents a first effort to assess nitrate simulation from chemical and physical
819 processes. A companion study is proposed by AeroCom III nitrate activity to investigate
820 how sensitive is nitrate formation in response to the possible future changes of emission
821 and meteorological fields. These perturbation fields include increasing NH_3 emission,
822 decreasing NO_x , SO_x and dust emissions, and increasing atmospheric temperature and
823 relative humidity. It would be particularly interesting to examine how aerosol pH changes
824 and its influence on atmospheric acid/base gas-particle system during the experiment.

825 Future aerosol pH does not necessarily increase with SO₂ emission reduction. Indeed,
 826 studies over US southeast indicated that its aerosol has been getting more acidic over the
 827 past decade although SO₂ emission decreased and NH₃ emission stayed constant [Silvern
 828 et al., 2017; Weber et al., 2016]. This environment of high aerosol acidity hinders the
 829 formation of nitrate aerosol, which only occurs when pH is over ~2 to 3 [Weber et al.,
 830 2016]. In addition, understanding why and how the system is insensitive to changing SO₂
 831 level due to buffering of the partitioning of semivolatile NH₃ over regions such as US
 832 southeast helps us to gain some insight into how errors in sulfate (and ammonium) may
 833 propagate to errors in aerosol nitrate. In particular, the correlation between model
 834 predictions and observations for SO₄²⁻ and NH₄⁺ is quite poor for some models (Figure 4).
 835 It would be also interesting to include organic gas/aerosol into the system since they are
 836 not only important atmospheric components, but also reduce the uptake of NH₃.
 837 Competition for uptake between NH₃ and organic gases considerably slows down the
 838 approach to thermodynamic equilibrium [Silvern et al., 2017]. Based on the findings of
 839 this work, modelers should pay particular attention to incorporating dust and sea salt and
 840 treating NH₃ wet deposition to improve nitrate simulation. Further evaluation using
 841 satellite measurements, such as NH₃ products from IASI and TES, is desired and will be
 842 conducted. Such evaluation requires global 3-dimensional high frequency model data.
 843 Potential future study also includes estimation of nitrate forcing for climate change.

844

845 **Appendix**

846 For some acidic/basic gases, including NH₃, Henry's law constant is also a function of
 847 pH in water (a.k.a effective Henry's law constant). This is because not only does the
 848 aqueous chemistry reaction NH₃ + H₂O (equation 1) reach equilibrium within a chemical
 849 time step but its product NH₃·H₂O (equation 2) does as well.



850 Here, NH₄⁺ is the ammonium ion and OH⁻ is the hydroxide ion. The total dissolved
 851 ammonia [NH₃^T] is given by

$$\begin{aligned} [NH_3^T] &= [NH_3 \cdot H_2O] + [NH_4^+] \\ &= p_{NH_3} H^\ominus \left(1 + \frac{K_{al}[H^+]}{K_w} \right) \\ &\approx p_{NH_3} \left(H^\ominus \frac{K_{al}[H^+]}{K_w} \right) \end{aligned} \quad (3)$$

852 Here, p_{NH₃} is the partial pressure of NH₃, K_{al} = [NH₄⁺][OH⁻] / [NH₃·H₂O] ≈ 1.8x10⁻⁵, and
 853 K_w = 1.0x10⁻¹⁴ at 298 K in pure water. So the effective Henry's law constant H^{⊖*} is
 854 inferred from H[⊖] with a correction of pH (pH = -log₁₀[H⁺]) as

$$H^{\ominus*} = H^\ominus \frac{K_{al}[H^+]}{K_w} \quad (4)$$

855

856 **References:**

857 Allen¹, H. M., D. C. Draper¹, B. R. Ayres, A. Ault, A. Bondy, S. Takahama, R. L. Modini, K. Baumann, E.
 858 Edgerton, C. Knote, A. Laskin, B. Wang, and J. L. Fry, Influence of crustal dust and sea spray
 859 supermicron particle concentrations and acidity on inorganic NO₃ aerosol during the 2013 Southern
 860 Oxidant and Aerosol Study, Atmos. Chem. Phys., 15, 10669–10685, 2015, [www.atmos-chem-](http://www.atmos-chem-phys.net/15/10669/2015/)
 861 [phys.net/15/10669/2015/](http://www.atmos-chem-phys.net/15/10669/2015/), doi:10.5194/acp-15-10669-2015.

862 Bauer, S. E., Balkanski, Y., Schulz, M., Hauglustaine, D. A., and Dentener, F.: Global modeling of
863 heterogeneous chemistry on mineral aerosol surfaces: Influence on tropospheric ozone chemistry and
864 comparison to observations, *J. Geophys. Res.-Atmos.*, 109, D02304, doi:10.1029/2003jd003868, 2004.
865 Bauer, S.E., and D. Koch, 2005: Impact of heterogeneous sulfate formation at mineral dust surfaces on
866 aerosol loads and radiative forcing in the Goddard Institute for Space Studies general circulation
867 model. *J. Geophys. Res.*, 110, D17202, doi:10.1029/2005JD005870.
868 Bauer, S. E., Koch, D., Unger, N., Metzger, S. M., Shindell, D. T., and Streets, D. G.: Nitrate aerosols
869 today and in 2030: a global simulation including aerosols and tropospheric ozone, *Atmos. Chem.*
870 *Phys.*, 7, 5043–5059, doi:10.5194/acp-7-5043-2007, 2007.
871 Bauer, S.E., D. Wright, D. Koch, E.R. Lewis, R. McGraw, L.-S. Chang, S.E. Schwartz, and R. Ruedy,
872 2008: MATRIX (Multiconfiguration Aerosol TRacker of mIXing state): An aerosol microphysical
873 module for global atmospheric models. *Atmos. Chem. Phys.*, 8, 6603-6035, doi:10.5194/acp-8-6003-
874 2008.
875 Bauer, S. E., K. Tsigaridis, and R. Miller, Significant atmospheric aerosol pollution caused by world food
876 cultivation, *Geophys. Res. Lett.*, 43, no. 10, 5394-5400, doi:10.1002/2016GL068354, 2016.
877 Bessagnet, B. and Rouil, L.: Feedback on and analysis of the PM pollution episode in March 2014,
878 presentation at 19-th EIONET Workshop on Air Quality Assessment and Management Berne,
879 Switzerland, 30 September and 1 October 2014, 2014.
880 Bey, I, D.J. Jacob, R.M. Yantosca, J.A. Logan, B.D. Field, A.M. Fiore, Q. Li, H.Y. Liu, L.J. Mickley, M.G.
881 Schultz, 2001: Global modeling of tropospheric chemistry with assimilated meteorology: Model
882 description and evaluation. *J. Geophys. Res.*, 106, 23073-23078 (2001JD000807).
883 Bellouin, N., Rae, J., Jones, A., Johnson, C., Haywood, J., and Boucher, O.: Aerosol forcing in the Climate
884 Model Intercomparison Project (CMIP5) simulations by HadGEM2-ES and the role of ammonium
885 nitrate, *J. Geophys. Res.-Atmos.*, 116, D20206, doi:10.1029/2011jd016074, 2011.
886 Berntsen, T. K. and Isaksen, I. S. A.: A global three-dimensional chemical transport model for the
887 troposphere. I. Model description and CO and ozone results, *J. Geophys. Res.-Atmos.*, 102(D17), 21
888 239–21 280, 1997.
889 Bian, H., and C. S. Zender (2003), Mineral dust and global tropospheric chemistry: The relative roles of
890 photolysis and heterogeneous uptake. *J. Geophys. Res.*, 108, 4672.
891 Bian, H., Chin, M., Rodriguez, J. M., Yu, H., Penner, J. E., and Strahan, S., 2009: Sensitivity of aerosol
892 optical thickness and aerosol direct radiative effect to relative humidity, *Atmos. Chem. Phys.*, 9, 2375-
893 2386, doi:10.5194/acp-9-2375-2009.
894 Bian, H., Colarco, P. R., Chin, M., Chen, G., Rodriguez, J. M., Liang, Q., Blake, D., Chu, D. A.,
895 da Silva, A., Darmenov, A. S., Diskin, G., Fuelberg, H. E., Huey, G., Kondo, Y., Nielsen, J. E.,
896 Pan, X., and Wisthaler, A.: Source attributions of pollution to the Western Arctic during the NASA
897 ARCTAS field campaign, *Atmos. Chem. Phys.*, 13, 4707-4721, doi:10.5194/acp-13-4707-2013, 2013.
898 Bouwman, A.F., Lee, D.S., Asman, W.A.H., Dentener, F.J., Van Der Hoek, K.W. and J.G.J. Olivier (1997).
899 A Global High-Resolution Emission Inventory for Ammonia, *Global Biogeochemical Cycles*, 11:4,
900 561-587. <http://www.rivm.nl/>.
901 Chin, M., P. Ginoux, S. Kinne, B. N. Holben, B. N. Duncan, R. V. Martin, J. A. Logan, A. Higurashi, and
902 T. Nakajima, 2002: Tropospheric aerosol optical thickness from the GOCART model and comparisons
903 with satellite and sun photometer measurements, *J. Atmos. Sci.* 59, 461-483.
904 Cubison, M.J., A.M. Ortega, P.L. Hayes, D.K. Farmer, D. Day, M.J. Lechner, W.H. Brune, E. Apel, G.S.
905 Diskin, J.A. Fisher, H.E. Fuelberg, A. Hecobian, D.J. Knapp, T. Mikoviny, D. Riemer, G.W. Sachse,
906 W. Sessions, R.J. Weber, A.J. Weinheimer, A. Wisthaler, and J.L. Jimenez (2011), Effects of Aging on
907 Organic Aerosol from Open Biomass Burning Smoke in Aircraft & Lab Studies. *Atmos. Chem. and*
908 *Phys. Disc.* 11, 12103-12140, doi:10.5194/acpd-11-12103-2011.
909 DeCarlo, P. F., Kimmel, J. R., Trimborn, A., Northway, M. J., Jayne, J. T., Aiken, A. C., Gonin, M.,
910 Fuhrer, K., Horvath, T., Docherty, K. S., Worsnop, D. R., and Jimenez, J. L.: Field-deployable, high-
911 resolution, time-of-flight aerosol mass spectrometer, *Anal. Chem.*, 78(24), 8281–8289, 2006.
912 Dentener, F. J., G. R. Carmichael, Y. Zhang, J. Lelieveld, and P. J. Crutzen, Role of mineral aerosol as a
913 reactive surface in the global troposphere, *J. Geophys. Res.*, 101, 22,869-22889, 1996.
914 Dentener, F., Kinne, S., Bond, T., Boucher, O., Cofala, J., Generoso, S., Ginoux, P., Gong, S., Hoelzemann,
915 J. J., Ito, A., Marelli, L., Penner, J. E., Putaud, J.-P., Textor, C., Schulz, M., van der Werf, G. R., and
916 Wilson, J.: Emissions of primary aerosol and precursor gases in the years 2000 and 1750 prescribed
917 data-sets for AeroCom, *Atmos. Chem. Phys.*, 6, 4321–4344, doi:10.5194/acp-6-4321-2006, 2006.

918 Ensberg, J. J., Craven, J. S., Metcalf, A. R., Allan, J. D., Angevine, W. M., Bahreini, R., Brioude, J., Cai,
919 C., Coe, H., de Gouw, J. A., Ellis, R. A., Flynn, J. H., Haman, C. L., Hayes, P. L., Jimenez, J. L.,
920 Lefer, B. L., Middlebrook, A. M., Murphy, J. G., Neuman, J. A., Nowak, J. B., Roberts, J. M., Stutz, J.,
921 Taylor, J. W., Veres, P. R., Walker, J. M., and Seinfeld, J. H.: Inorganic and black carbon aerosols in
922 the Los Angeles Basin during CalNex, *Journal of Geophysical Research-Atmospheres*, 118, 1777-
923 1803, 2013.

924 Fairlie, T. D., Jacob, D. J., Dibb, J. E., Alexander, B., Avery, M. A., van Donkelaar, A., and Zhang, L.:
925 Impact of mineral dust on nitrate, sulfate, and ozone in transpacific Asian pollution plumes, *Atmos.*
926 *Chem. Phys.*, 10, 3999–4012, doi:10.5194/acp-10-3999-2010, 2010.

927 Feng, Y. and Penner, J. E.: Global modeling of nitrate and ammonium: Interaction of aerosols and
928 tropospheric chemistry, *J. Geophys. Res.-Atmos.*, 112, D01304, doi:10.1029/2005jd006404, 2007.

929 Fenn, M. E., M. A. Poth, D. W. Johnson, Evidence for nitrogen saturation in the San Bernardino Mountains
930 in southern California, *Forest Ecology and Management*, Volume 82, Issues 1–3, April 1996, Pages
931 211-230.

932 Fitzgerald, J. W. (1975), Approximation formulas for equilibrium size of an aerosol particle as a function
933 of its dry size and composition and ambient relative humidity, *J. Appl. Meteorol.*, 14(6), 1044-1049.

934 Fowler, Z. K., M. B. Adams, W. T. Peterjohn, Will more nitrogen enhance carbon storage in young forest
935 stands in central Appalachia? *Forest Ecology and Management*, Volume 337, Pages 144–152, 1
936 February 2015.

937 Galloway, J. N., Dentener, F. J., Capone, D. G., Boyer, E. W., Howarth, R. W., Seitzinger, S. P., Asner, G.
938 P., Cleveland, C. C., Green, P. A., Holland, E. A., Karl, D. M., Michaels, A. F., Porter, J. H.,
939 Townsend, A. R. and Vorosmarty, C. J.: Nitrogen cycles: Past, present, and future, *Biogeochemistry*,
940 70, 153–226, 2004.

941 Ginoux, P., M. Chin, I. Tegen, J. Prospero, B. Holben, O. Dubovik, and S.-J. Lin, 2001: Sources and global
942 distributions of dust aerosols simulated with the GOCART model, *J. Geophys. Res.*, 106, 20,255-
943 20,273.

944 Grieshop, A. P., Robinson, A. L., Duplissy, J., Smith, J. D., Wilson, K. R., Lanz, V. A., Hueglin, C., Sun,
945 Y. L., Tian, J., Laaksonen, A., Raatikainen, T., Rautiainen, J., Vaattovaara, P., Ehn, M., Kulmala, M.,
946 Tomlinson, J. M., Collins, D. R., Cubison, M. J., Dunlea, E. J., Huffman, J. A., Onasch, T. B., Alfarra,
947 M. R., Williams, P. I., Bower, K., Kondo, Y., Schneider, J., Drewnick, F., Borrmann, S., Weimer, S.,
948 Demerjian, K., Salcedo, D., Cottrell, L., Griffin, R., Takami, A., Miyoshi, T., Hatakeyama, S.,
949 Shimono, A., Sun, J. Y., Zhang, Y. M., Dzepina, K., Kimmel, J. R., Sueper, D., Jayne, J. T., Herndon,
950 S. C., Trimborn, A. M., Williams, L. R., Wood, E. C., Middlebrook, A. M., Kolb, C. E., Baltensperger,
951 U., and Worsnop, D. R.: Evolution of organic aerosols in the atmosphere, *Science*, 326, 1525–1529,
952 2009.

953 Hansell, D.A., Follows, M.J., 2008. Nitrogen in the Atlantic Ocean. In: Mullholland, M., Bronk, D.,
954 Capone, D., Carpenter, E. (Eds.), *Nitrogen in the Marine Environment*, second ed. Academic Press, pp.
955 597–630.

956 Hauglustaine, D. A., Hourdin, F., Walters, S., Jourdain, L., Filiberti, M.-A., Lamarque, J.-F., and Holland,
957 E. A.: Interactive chemistry in the Laboratoire de Météorologie Dynamique general circulation model:
958 description and background tropospheric chemistry evaluation, *J. Geophys. Res.*, 109, D04314,
959 doi:10.1029/2003JD003957, 2004.

960 Hauglustaine, D. A., Balkanski, Y., and Schulz, M.: A global model simulation of present and future
961 nitrate aerosols and their direct radiative forcing of climate, *Atmos. Chem. Phys.*, 14, 11031–11063,
962 doi:10.5194/acp-14-11031-2014, 2014.

963 Haywood, J., Bush, M., Abel, S., Claxton, B., Coe, H., Crosier, J., Harrison, M., Macpherson, B., Naylor,
964 M., and Osborne, S.: Prediction of visibility and aerosol within the operational Met Office Unified
965 Model II?: Validation of model performance using observational data, *Q. J. Roy. Meteorol. Soc.*, 134,
966 1817–1832, doi:10.1002/qj.275, 2008.

967 Heald, C. L., Collett Jr., J. L., Lee, T., Benedict, K. B., Schwandner, F. M., Li, Y., Clarisse, L., Hurtmans,
968 D. R., Van Damme, M., Clerbaux, C., Coheur, P.-F., Philip, S., Martin, R. V., and Pye, H. O. T.:
969 Atmospheric ammonia and particulate inorganic nitrogen over the United States, *Atmos. Chem. Phys.*,
970 12, 10295–10312, doi:10.5194/acp-12-10295-2012, 2012.

971 Hess, M., P. Koepke and I. Schult, Optical properties of aerosols and clouds: The software package OPAC.
972 *Bull. Amer. Meteorol. Soc.*, 79(5): 831-844, 1998.

973 Huffman, J. A., J. T. Jayne, F. Drewnick, A. C. Aiken, T. Onasch, D. R. Worsnop, and J. L. Jimenez,
 974 Design, Modeling, Optimization, and Experimental Tests of a Particle Beam Width Probe for the
 975 Aerodyne Aerosol Mass Spectrometer, *Aerosol Sci Technol.* 39, 1143-1163, 2005.
 976 Huneeus, N., M. Schulz, Y. Balkanski, J. Griesfeller, S. Kinne, J. Prospero, S. Bauer, O. Boucher, M. Chin,
 977 F. Dentener, T. Diehl, R. Easter, D. Fillmore, S. Ghan, P. Ginoux, A. Grini, L. Horowitz, D. Koch,
 978 M.C. Krol, W. Landing, X. Liu, N. Mahowald, R.L. Miller, J.-J. Morcrette, G. Myhre, J.E. Penner, J.P.
 979 Perlwitz, P. Stier, T. Takemura, and C. Zender, 2011: Global dust model intercomparison in AeroCom
 980 phase I. *Atmos. Chem. Phys.*, 11, 7781-7816, doi:10.5194/acp-11-7781-2011.
 981 IPCC: (Intergovernmental Panel on Climate Change): The physical science basis. Contribution of working
 982 group I to the fifth assessment report of the intergovernmental panel on climate change. T.F. Stocker, D.
 983 Qin, G.-K. Plattner, M. Tignor, S.K. Allen, J. Boschung, A. Nauels, Y. Xia, V. Bex, and P.M. Midgley
 984 (eds.). Cambridge University Press, Cambridge, United Kingdom and New York, NY, USA, 2013.
 985 2013.
 986 Jimenez, J. L., Canagaratna, M. R., Donahue, N. M., Prevot, A. S. H., Zhang, Q., Kroll, J. H., DeCarlo, P.
 987 F., Allan, J. D., Coe, H., Ng, N. L., Aiken, A. C., Docherty, K. S., Ulbrich, I. M.,
 988 Jacob, D. J., Crawford, J. H., Mering, H., Clarke, A. D., Dibb, J. E., Emmons, L. K., Ferrare, R. A.,
 989 Hostetler, C. A., Russell, P. B., Singh, H. B., Thompson, A. M., Shaw, G. E., McCauley, E., Pederson,
 990 J. R., and Fisher, J. A.: The Arctic Research of the Composition of the Troposphere from Aircraft and
 991 Satellites (ARCTAS) mission: design, execution, and first results, *Atmos. Chem. Phys.*, 10, 5191–
 992 5212, doi:10.5194/acp-10-5191-2010, 2010.
 993 Janssens-Maenhout, G., Crippa, M., Guizzardi, D., Dentener, F., Muntean, M., Pouliot, G., Keating, T.,
 994 Zhang, Q., Kurokawa, J., Wankmüller, R., Denier van der Gon, H., Kuenen, J. J. P., Klimont, Z., Frost,
 995 G., Darras, S., Koffi, B., and Li, M.: HTAP_v2.2: a mosaic of regional and global emission grid maps
 996 for 2008 and 2010 to study hemispheric transport of air pollution, *Atmos. Chem. Phys.*, 15, 11411–
 997 11432, doi:10.5194/acp-15-11411-2015, 2015
 998 Jöckel, P., Kerkweg, A., Pozzer, A., Sander, R., Tost, H., Riede, H., Baumgaertner, A., Gromov, S., and
 999 Kern, B.: Development cycle 2 of the Modular Earth Submodel System (MESSy2), *Geosci. Model
 1000 Dev.*, 3, 717–752, doi:10.5194/gmd-3-717-2010, 2010.
 1001 John, W., S. M. Wall, J. L. Ondo, and W. Winklmayr (1989), Acidic-aerosol size distributions during
 1002 SCAQS (Southern California Air Quality Study), final report, Rep. CA/DOH/AIHL/SP-51, Calif. Air
 1003 Resour. Board, Sacramento.
 1004 Kanakidou, M., R.A. Duce, J.M. Prospero, A.R. Baker, C. Benitez-Nelson, F.J. Dentener, K.A. Hunter,
 1005 P.S. Liss, N. Mahowald, G.S. Okin, M. Sarin, K. Tsigaridis, M. Uematsu, L.M. Zamora, and T. Zhu,
 1006 2012: Atmospheric fluxes of organic N and P to the global ocean. *Glob. Biogeochem. Cycles*, 26,
 1007 GB3026, doi:10.1029/2011GB004277.
 1008 Kanakidou, M., S. Myriokefalitakis, N. Daskalakis, G. Fanourgakis, A. Nenes, A. Baker, K. Tsigaridis, and
 1009 N. Mihalopoulos, 2016: Past, present and future atmospheric nitrogen deposition. *J. Atmos. Sci.*, 73,
 1010 no. 5, 2039-2047, doi:10.1175/JAS-D-15-0278.1.
 1011 Karydis, V. A., Tsimpidi, A. P., Fountoukis, C., Nenes, A., Zavala, M., Lei, W., Molina, L. T., and Pandis,
 1012 S. N.: Simulating the fine and coarse inorganic particulate matter concentrations in a polluted
 1013 megacity, *Atmospheric Environment*, 44, 608-620, 2010.
 1014 Karydis, V. A., Tsimpidi, A. P., Lei, W., Molina, L. T., and Pandis, S. N.: Formation of semivolatile
 1015 inorganic aerosols in the Mexico City Metropolitan Area during the MILAGRO campaign,
 1016 *Atmospheric Chemistry and Physics*, 11, 13305-13323, 2011.
 1017 Karydis, V. A., A. P. Tsimpidi, A. Pozzer, M. Astitha, and J. Lelieveld, 2016: Effects of mineral dust on
 1018 global atmospheric nitrate concentrations. *Atmos. Chem. Phys.*, 16, 1491–1509, doi:10.5194/acp-16-
 1019 1491-2016.
 1020 Kim, Y. P., Seinfeld, J. H., and Saxena, P.: Atmospheric gas–aerosol equilibrium I. Thermodynamic model,
 1021 *Aerosol Sci. Technol.*, 19, 157–181, 1993.
 1022 Kim, D., M. Chin, H. Yu, T. Diehl, Q. Tan, R.A. Kahn, K. Tsigaridis, S.E. Bauer, T. Takemura, L. Pozzoli,
 1023 N. Bellouin, M. Schulz, S. Peyridieu, A. Chédin, and B. Koffi, 2014: Sources, sinks, and transatlantic
 1024 transport of North African dust aerosol: A multi-model analysis and comparison with remote-sensing
 1025 data. *J. Geophys. Res. Atmos.*, 119, no. 10, 6259-6277, doi:10.1002/2013JD021099.
 1026 Kinne, S., Schulz, M., Textor, C., Guibert, S., Balkanski, Y., Bauer, S. E., Berntsen, T., Berglen, T. F.,
 1027 Boucher, O., Chin, M., Collins, W., Dentener, F., Diehl, T., Easter, R., Feichter, J., Fillmore, D., Ghan,
 1028 S., Ginoux, P., Gong, S., Grini, A., Hendricks, J., Herzog, M., Horowitz, L., Isaksen, I., Iversen, T.,

1029 Kirkevåg, A., Kloster, S., Koch, D., Kristjansson, J. E., Krol, M., Lauer, A., Lamarque, J. F., Lesins,
1030 G., Liu, X., Lohmann, U., Montanaro, V., Myhre, G., Penner, J., Pitari, G., Reddy, S., Seland, O.,
1031 Stier, P., Takemura, T., and Tie, X.: An AeroCom initial assessment – optical properties in aerosol
1032 component modules of global models, *Atmos. Chem. Phys.*, 6, 1815–1834, doi:10.5194/acp-6-1815-
1033 2006, 2006.

1034 Koch, D., M. Schulz, S. Kinne, C. McNaughton, J.R. Spackman, T.C. Bond, Y. Balkanski, S. Bauer, T.
1035 Berntsen, O. Boucher, M. Chin, A. Clarke, N. De Luca, F. Dentener, T. Diehl, O. Dubovik, R. Easter,
1036 D.W. Fahey, J. Feichter, D. Fillmore, S. Freitag, S. Ghan, P. Ginoux, S. Gong, L. Horowitz, T. Iversen,
1037 A. Kirkevåg, Z. Klimont, Y. Kondo, M. Krol, X. Liu, R.L. Miller, V. Montanaro, N. Moteki, G.
1038 Myhre, J.E. Penner, J.P. Perlwitz, G. Pitari, S. Reddy, L. Sahu, H. Sakamoto, G. Schuster, J.P.
1039 Schwarz, Ø. Seland, P. Stier, N. Takegawa, T. Takemura, C. Textor, J.A. van Aardenne, and Y. Zhao,
1040 2009: Evaluation of black carbon estimations in global aerosol models. *Atmos. Chem. Phys.*, 9, 9001-
1041 9026, doi:10.5194/acp-9-9001-2009.

1042 Kinnison, D. E., P. S. Connell, J. Rodriguez, D. B. Considine, D. A. Rotman, J. Tannahill, R. Ramaroson,
1043 A. Douglass, S. Baughcum, L. Coy, P. Rasch, D. Waugh, 2001: The Global Modeling Initiative
1044 assessment model: Application to high-speed civil transport perturbation, *J. Geophys. Res.*, 106, 1693-
1045 1712.

1046 Lacis, A. A., Refractive Indices of Three Hygroscopic Aerosols and their Dependence on Relative
1047 Humidity, http://gacp.giss.nasa.gov/data_sets/lacis/introduction.pdf.

1048 Lamarque, J.-F., J. T. Kiehl, G. P. Brasseur, T. Butler, P. Cameron-Smith, et al. (2005), Assessing future
1049 nitrogen deposition and carbon cycle feedback using a multimodel approach : Analysis of nitrogen
1050 deposition, *J. of Geophys. Res.*, Vol. 110, D19303, doi: 10.1029/2005JD005825.

1051 Lee, T., X.-Y. Yu, B. Ayres, S. M. Kreidenweis, W. C. Malm, J. L. Collett Jr., Observations of fine and
1052 coarse particle nitrate at several rural locations in the United States, *Atmospheric Environment* 42,
1053 2720–2732, 2008.

1054 Li, J., W.-C. Wang, H. Liao, and W. Chang. 2014. Past and future direct radiative forcing of nitrate aerosol
1055 in East Asia. *Theor. Appl. Climatol.* 1–14. doi:10.1007/s00704-014-1249-1.

1056 Liao, H., P. J. Adams, S. H. Chung, J. H. Seinfeld, L. J. Mickley, and D. J. Jacob (2003), Interactions
1057 between tropospheric chemistry and aerosols in a unified general circulation model, *J. Geophys. Res.*,
1058 108(D1), 4001, doi:10.1029/2001JD001260.

1059 Liu, X., J. E. Penner, S. J. Ghan, and M. Wang, 2007: Inclusion of Ice Microphysics in the NCAR
1060 Community Atmospheric Model Version 3 (CAM3). *J. Climate*, 20, 4526-4547.

1061 Liu, Y., G. Gibson, C. Cain, H. Wang, G. Grassian, and A. Laskin (2008) Kinetics of Heterogeneous
1062 Reaction of CaCO₃ Particles with Gaseous HNO₃ over a Wide Range of Humidity, *J. Physical
1063 Chemistry A*, doi:10.1021/jp076169h

1064 Malm, W. C., Schichtel, B. A., Pitchford, M. L., Ashbaugh, L. L., and Eldred, R. A.: Spatial and monthly
1065 trends in speciated fine particle concentration in the United States, *J. Geophys. Res. Atmos.*, 109(D3),
1066 D03306, doi:10.1029/2003/JD003739, 2004.

1067 Metzger, S., F. Dentener, S. Pandis, and J. Lelieveld (2002), Gas/aerosol partitioning: 1. A computationally
1068 efficient model, *J. of Geophys. Res.* Vol. 107, No. D16, 4312, 10.1029/2001JD001102.

1069 Mezuman, K., S.E. Bauer, and K. Tsigaridis, 2016: Evaluating secondary inorganic aerosols in three
1070 dimensions. *Atmos. Chem. Phys.*, 16, 10651-10669, doi:10.5194/acp-16-10651-2016.

1071 Milegroet, H. Van and D. W. Cole, The Impact of Nitrification on Soil Acidification and Cation Leaching
1072 in a Red Alder Ecosystem, ACSESS, Alliance of Crop, Soil, and Environmental Science Societies,
1073 doi:10.2134/jeq1984.00472425001300040015x ,1984

1074 Myhre, G., A. Grini, and S. Metzger (2006), Modeling of nitrate and ammonium-containing aerosols
1075 in presence of sea salt, *Atmos. Chem. Phys.*, 6, 4809-4821, www.atmos-chem-phys.net/6/4809/2006/.

1076 Myhre, G., B. H., Samsset, M. Schulz, Y. Balkanski, S. Bauer, T. K. Berntsen, H. Bian, N. Bellouin, M.
1077 Chin, T. Diehl, R. C. Easter, J. Feichter, S. J. Ghan, D. Hauglustaine, T. Iversen, S. Kinne, A.
1078 Kirkevåg, J.-F. Lamarque, G. Lin, X. Liu, G. Luo, X. Ma, J. E. Penner, P. J. Rasch, Ø. Seland, R. B.
1079 Skeie, P. Stier, T. Takemura, K. Tsigaridis, Z. Wang, L. Xu, H. Yu, F. Yu, J.-H. Yoon, K. Zhang, H.
1080 Zhang, and C. Zhou, Radiative forcing of the direct aerosol effect from AeroCom Phase II simulations,
1081 *Atmos. Chem. Phys.*, 13, 1853-1877, doi:10.5194/acp-13-1853-2013, 2013.

1082 Nowak, J., J. B., Weinheimer, A. J., Hoff, R. M., Berkoff, T. A., Beyersdorf, A. J., Olson, J., Crawford, J.
1083 H., and Cohen, R. C.: On the effectiveness of nitrogen oxide reductions as a control over ammonium
1084 nitrate aerosol, *Atmos. Chem. Phys.*, 16, 2575–2596, doi:10.5194/acp-16-2575-2016, 2016

1085 Paulot, F., Ginoux, P., Cooke, W. F., Donner, L. J., Fan, S., Lin, M.-Y., Mao, J., Naik, V., and Horowitz, L.
1086 W.: Sensitivity of nitrate aerosols to ammonia emissions and to nitrate chemistry: implications for
1087 present and future nitrate optical depth, *Atmos. Chem. Phys.*, 16, 1459–1477, doi:10.5194/acp-16-
1088 1459-2016, <http://www.atmos-chem-phys.net/16/1459/2016/>, 2016.

1089 Phoenix, G., W. K. Hicks, S. Cinderby, J. C. I. Kuylentierna, W. D. Stock, et al. (2006), Atmospheric
1090 nitrogen deposition in world biodiversity hotspots: the need for a greater global perspective in
1091 assessing N deposition impacts, *Global Change Biology*, 12, 470-476, doi: 10.1111/j.1365-
1092 2486.2006.01104.x.

1093 Prentice, M. J., et al. (2001), The carbon cycle and atmospheric carbon dioxide, in *Climate Change 2001*,
1094 pp. 184-237, Cambridge Univ. Press, New York.

1095 Pringle, K. J., Tost, H., Message, S., Steil, B., Giannadaki, D., Nenes, A., Fountoukis, C., Stier, P., Vignati,
1096 E., and Leueved, J.: Description and evaluation of GMXe: a new aerosol submodel for global
1097 simulations (v1), *Geoscientific Model Development*, 3, 391-412, 2010.

1098 Pusede, S. E., Duffey, K. C., Shusterman, A. A., Saleh, A., Laughner, J. L., Wooldridge, P. J., Zhang, Q.,
1099 Parworth, C. L., Kim, H., Capps, S. L., Valin, L. C., Cappa, C. D., Fried, A., Walega, Riemer, N., H.
1100 Vogel, B. Vogel, B. Schell, I. Ackermann, C. Kessler, and H. Hass (2003), Impact of the
1101 heterogeneous hydrolysis of N₂O₅ on chemistry and nitrate aerosol formation in the lower troposphere
1102 under photosmog conditions, *J. Geophys. Res.*, 108(D4), 4144, doi:10.1029/2002JD002436.

1103 Sander, S. P., J. Abbatt, J. R. Barker, J. B. Burkholder, R. R. Friedl, D. M. Golden, R. E. Huie, C. E. Kolb,
1104 M. J. Kurylo, G. K. Moortgat, V. L. Orkin and P. H. Wine "Chemical Kinetics and Photochemical
1105 Data for Use in Atmospheric Studies, Evaluation No. 17," JPL Publication 10-6, Jet Propulsion
1106 Laboratory, Pasadena, 2011 <http://jpldataeval.jpl.nasa.gov>.

1107 Saxena, P., Hudischevskyj, A. B., Seigneur, C., and Seinfeld, J. H., A comparative study of
1108 equilibrium approaches to the chemical characterization of secondary aerosols, *Atmos. Environ.*
1109 20:1471- 1483, 1986.

1110 Schaap, M., Müller, K., & Ten Brink, H. M. (2002). Constructing the European aerosol nitrate
1111 concentration field from quality analysed data. *Atmospheric Environment*, 36(8), 1323-1335.

1112 Schaap, M., van Loon, M., ten Brink, H. M., Dentener, F. J., and Builtjes, P. J. H.: Secondary
1113 inorganic aerosol simulations for Europe with special attention to nitrate, *Atmos. Chem. Phys.*, 4,
1114 857-874, doi:10.5194/acp-4-857-2004, 2004.

1115 Schmidt, G.A., M. Kelley, L. Nazarenko, R. Ruedy, G.L. Russell, I. Aleinov, M. Bauer, S.E. Bauer,
1116 M.K. Bhat, R. Bleck, V. Canuto, Y.-H. Chen, Y. Cheng, T.L. Clune, A. Del Genio, R. de
1117 Fainchtein, G. Faluvegi, J.E. Hansen, R.J. Healy, N.Y. Kiang, D. Koch, A.A. Lacis, A.N.
1118 LeGrande, J. Lerner, K.K. Lo, E.E. Matthews, S. Menon, R.L. Miller, V. Oinas, A.O. Oloso, J.P.
1119 Perlwitz, M.J. Puma, W.M. Putman, D. Rind, A. Romanou, M. Sato, D.T. Shindell, S. Sun, R.A.
1120 Syed, N. Tausnev, K. Tsigaridis, N. Unger, A. Voulgarakis, M.-S. Yao, and J. Zhang, 2014:
1121 Configuration and assessment of the GISS ModelE2 contributions to the CMIP5 archive. *J. Adv.*
1122 *Model. Earth Syst.*, 6, no. 1, 141-184, doi:10.1002/2013MS000265.

1123 Schulz, M., Textor, C., Kinne, S., Balkanski, Y., Bauer, S., Bernsten, T., Berglen, T., Boucher, O.,
1124 Dentener, F., Guibert, S., Isaksen, I. S. A., Iversen, T., Koch, D., Kirkevåg, A., Liu, X.,
1125 Montanaro, V., Myhre, G., Penner, J. E., Pitari, G., Reddy, S., Seland, Ø., Stier, P., and
1126 Takemura, T.: Radiative forcing by aerosols as derived from the AeroCom present-day and pre-
1127 industrial simulations, *Atmos. Chem. Phys.*, 6, 5225–5246, doi:10.5194/acp-6-5225-2006, 2006.

1128 Schutgens, N. A. J., Gryspeerdt, E., Weigum, N., Tsyro, S., Goto, D., Schulz, M. and Stier, P.: Will a
1129 perfect model agree with perfect observations? The impact of spatial sampling, *Atmos. Chem.*
1130 *Phys.*, 16(10), 6335-6353, 2016.

1131 Shindell, D. T., Faluvegi, G., and Bell, N.: Preindustrial-to-present-day radiative forcing by
1132 tropospheric ozone from improved simulations with the GISS chemistry-climate GCM, *Atmos.*
1133 *Chem. Phys.*, 3, 1675–1702, 2003.

1134 [Silvern, R. F., Jacob, D. J., Kim, P. S., Marais, E. A., Turner, J. R., Campuzano-Jost, P., and](#)
1135 [Jimenez, J. L.: Inconsistency of ammonium–sulfate aerosol ratios with thermodynamic](#)
1136 [models in the eastern US: a possible role of organic aerosol, *Atmos. Chem. Phys.*, 17, 5107-](#)
1137 [5118, 10.5194/acp-17-5107-2017, 2017.](#)

1138 Simpson, D., Benedictow, A., Berge, H., Bergström, R., Emberson, L. D., Fagerli, H., Flechard, C. R.,

1139 Hayman, G. D., Gauss, M., Jonson, J. E., Jenkin, M. E., Nyíri, A., Richter, C., Semeena, V. S., Tsyro,
 1140 S., Tuovinen, J. P., Valdebenito, Á., and Wind, P.: The EMEP MSC-W chemical transport model -
 1141 technical description, *Atmos. Chem. Phys.*, 12, 7825-7865, 10.5194/acp-12-7825-2012, 2012.
 1142 Song, C. H., and G. R. Carmichael, Gas-particle partitioning of nitric acid modulated by alkaline aerosol, *J.*
 1143 *Atmos. Chem.*, 40, 1–22, 2001.
 1144 Strahan, S. E., Duncan, B. N., and Hoor, P.: Observationally derived transport diagnostics for the
 1145 lowermost stratosphere and their application to the GMI chemistry and transport model, *Atmos. Chem.*
 1146 *Phys.*, 7, 2435-2445, doi:10.5194/acp-7-2435-2007, 2007.
 1147 Sudo, K., M. Takahashi, J. Kurokawa, and H. Akimoto, CHASER: A global chemical model of the
 1148 troposphere, 1. Model description, *J. Geophys. Res.*, 107(D17), 4339, doi:10.1029/2001JD001113,
 1149 2002.
 1150 Takiguchi, Y., A. Takami, Y. Sadanaga, X. Lun, A. Shimizu, I. Matsui, N. Sugimoto, W. Wang, H.
 1151 Bandow, and S. Hatakeyama (2008), Transport and transformation of total reactive nitrogen over the
 1152 East China Sea, *J. Geophys. Res.*, 113, D10306, doi:10.1029/2007JD009462.
 1153 Textor, C., Schulz, M., Guibert, S., Kinne, S., Balkanski, Y., Bauer, S., Bernsten, T., Berglen, T., Boucher,
 1154 O., Chin, M., Dentener, F., Diehl, T., Easter, R., Feichter, H., Fillmore, D., Ghan, S., Ginoux, P.,
 1155 Gong, S., Grini, A., Hendricks, J., Horowitz, L., Huang, P., Isaksen, I., Iversen, I., Kloster, S., Koch,
 1156 D., Kirkevåg, A., Kristjansson, J. E., Krol, M., Lauer, A., Lamarque, J. F., Liu, X., Montanaro, V.,
 1157 Myhre, G., Penner, J., Pitari, G., Reddy, S., Seland, Ø., Stier, P., Takemura, T., and Tie, X.: Analysis
 1158 and quantification of the diversities of aerosol life cycles within AeroCom, *Atmos. Chem. Phys.*, 6,
 1159 1777–1813, doi:10.5194/acp-6-1777-2006, 2006.
 1160 Tost, H., Jöckel, P., Kerkweg, A., Sander, R., and Lelieveld, J.: Technical note: A new comprehensive
 1161 SCAVenging submodel for global atmospheric chemistry modelling, *Atmos. Chem. Phys.*, 6, 565-574,
 1162 doi:10.5194/acp-6-565-2006, 2006.
 1163 Trail, M., Tsimpidi, A. P., Liu, P., Tsigaridis, K., Rudokas, J., Miller, P., Nenes, A., Hu, Y., and Russell, A.
 1164 G.: Sensitivity of air quality to potential future climate change and emissions in the United States and
 1165 major cities, *Atmospheric Environment*, 94, 552-563, 2014.
 1166 Trump, E. R., Fountoukis, C., Donahue, N. M., and Pandis, S. N.: Improvement of simulation of fine
 1167 inorganic PM levels through better descriptions of coarse particle chemistry, *Atmospheric*
 1168 *Environment*, 102, 274-281, 2015.
 1169 Tsigaridis, K., Daskalakis, N., Kanakidou, M., Adams, P. J., Artaxo, P., Bahadur, R., Balkanski, Y.,
 1170 Bauer, S. E., Bellouin, N., Benedetti, A., Bergman, T., Bernsten, T. K., Beukes, J. P., Bian, H.,
 1171 Carslaw, K. S., Chin, M., Curci, G., Diehl, T., Easter, R. C., Ghan, S. J., Gong, S. L., Hodzic, A.,
 1172 Hoyle, C. R., Iversen, T., Jathar, S., Jimenez, J. L., Kaiser, J. W., Kirkevåg, A., Koch, D., Kokkola, H.,
 1173 Lee, Y. H., Lin, G., Liu, X., Luo, G., Ma, X., Mann, G. W., Mihalopoulos, N., Morcrette, J.-J.,
 1174 Müller, J.-F., Myhre, G., Myriokefalitakis, S., Ng, N. L., O'Donnell, D., Penner, J. E., Pozzoli, L.,
 1175 Pringle, K. J., Russell, L. M., Schulz, M., Sciare, J., Seland, Ø., Shindell, D. T., Sillman, S.,
 1176 Skeie, R. B., Spracklen, D., Stavrakou, T., Steenrod, S. D., Takemura, T., Tiitta, P., Tilmes, S.,
 1177 Tost, H., van Noije, T., van Zyl, P. G., von Salzen, K., Yu, F., Wang, Z., Wang, Z., Zaveri, R. A.,
 1178 Zhang, H., Zhang, K., Zhang, Q., and Zhang, X.: The AeroCom evaluation and intercomparison of
 1179 organic aerosol in global models, *Atmos. Chem. Phys.*, 14, 10845-10895, doi:10.5194/acp-14-10845-
 1180 2014, 2014.
 1181 Tsimpidi, A. P., Karydis, V. A., and Pandis, S. N.: Response of inorganic fine particulate matter to
 1182 emission changes of sulfur dioxide and ammonia: The eastern United States as a case study, *Journal of*
 1183 *the Air & Waste Management Association*, 57, 1489-1498, 2007.
 1184 Tsimpidi, A. P., Karydis, V. A., and Pandis, S. N.: Response of Fine Particulate Matter to Emission
 1185 Changes of Oxides of Nitrogen and-Anthropogenic Volatile Organic Compounds in the Eastern United
 1186 States, *Journal of the Air & Waste Management Association*, 58, 1463-1473, 2008.
 1187 Vieno, M., Heal, M. R., Twigg, M. M., MacKenzie, I. A., Braban, C. F., Lingard, J. J. N. Ritchie, S., Beck,
 1188 R. C., A. M., Ots, R., DiMarco, C. F., Nemitz, E., Sutton, M. A., and Reis, S.: The UK particulate
 1189 matter air pollution episode of March-April 2014: more than Saharan dust., *Environ. Res. Lett.*,
 1190 doi:10.1088/1748-9326/11/4/044004, 2016.
 1191 Walker, J. M., Philip, S., Martin, R. V., and Seinfeld, J. H.: Simulation of nitrate, sulfate, and ammonium
 1192 aerosols over the United States, *Atmos. Chem. Phys.*, 12, 11213–11227, doi:10.5194/acp-12-11213-
 1193 2012, 2012.

1194 Watanabe, S., T. Hajima, K. Sudo, T. Nagashima, T. Takemura, H. Okajima, *et al.* MIROC-ESM 2010:
1195 model description and basic results of CMIP5-20c3m experiments, *Geosci. Model Dev.*, 4 (2011), pp.
1196 845–872.
1197 [Weber, R. J., Guo, H., Russell, A. G., and Nenes, A.: High aerosol acidity despite declining](#)
1198 [atmospheric sulfate concentrations over the past 15 years, *Nature Geosci.*, 9, 282-285,](#)
1199 [10.1038/ngeo2665, 2016.](#)
1200 Williams, E. J., S. T. Sandholm, J. D. Bradshaw, J. S. Schendel, A. O. Langford, P. K. Quinn, P. J. LeBel,
1201 S. A. Vay, P. D. Roberts, R. B. Norton, B. A. Watkins, M. P. Buhr, D. D. Parrish, J. G. Calvert, and F.
1202 C. Fehsenfeld, An intercomparison of five ammonia measurement techniques, *J. Geophys. Res.*, Vol.,
1203 97, No. D11, Pages 11591-11611, July 20, 1992.
1204 van der Werf, G. R., Randerson, J. T., Giglio, L., Collatz, G. J., Mu, M., Kasibhatla, P. S., Morton, D. C.,
1205 DeFries, R. S., Jin, Y., and van Leeuwen, T. T.: Global fire emissions and the contribution of
1206 deforestation, savanna, forest, agricultural, and peat fires (1997–2009), *Atmos. Chem. Phys.*, 10,
1207 11707-11735, doi:10.5194/acp-10-11707-2010, 2010.
1208 Zender, C. S., Bian, H. S., and Newman, D.: Mineral Dust Entrainment and Deposition (DEAD) model:
1209 Description and 1990s dust climatology, *J. Geophys. Res.-Atmos.*, 108, 4416,
1210 doi:10.1029/2002jd002775, 2003.
1211 Zhou, J., B. Gu, W. H. Schlesinger, X. Ju, Significant accumulation of nitrate in Chinese semi-humid
1212 croplands, *Scientific Reports* 6, Article number: 25088, doi:10.1038/srep25088, 2016.

1213
1214
1215
1216
1217
1218
1219
1220
1221
1222
1223
1224
1225
1226
1227
1228
1229
1230
1231
1232
1233
1234
1235

Table 1. Nitrate chemical mechanism and physical properties of AeroCom models

Model	CHEM-EQM	HNO3 chem mechanism	CHEM DUST	CHEM SEASALT	How do CHEMDUSS	Bins for nitrate	Model Name & resolution	References
CHASER	ISORROPIA-I	CHASER (Sudo et al., 2002)	No	No	---	Fine mode	MIROC, GCM, 2.8°x2.8°x64	Watanabe et al., 2011
EMAC	ISORROPIA-II (Stable state ^a)	MESSy2 (Jöckel et al., 2010)	Yes	Yes	ISORROPIA-II	4 bins: Nucleation, Aitken, Accumulation, Coarse	ECHAM5, GCM, 2.8°x2.8°x31	Karydis et al., 2016
EMEP	MARS	EMEP EmChem09	Yes	Yes	First order	Fine and	ECMWF-IFS,	Simpson et

Formatted: Superscript

		(Simpson et al., 2012)			loss	coarse	CTM, 0.5x0.5x20	al., 2012
GMI	RPMARES (Stable state)	GMI (Straham et al., 2007)	Yes	Yes	first order loss	3 bins; (D<0.1, 0.1 - 2.5, > 2.5 um)	MERRA2, CTM, 2.5x2.5x72	Bian et al., 2009
INCA	INCA (Stable state)	INCA tropospheric chemistry (Hauglustaine et al., 2004)	Yes	Yes	first order loss	2 bins : (D< 1µm and 1 - 10µm)	LMD-v4, GCM, 1.9x3.75x39	Hauglustaine et al., 2014
GISS MATRIX	ISORROPIA-II (Stable state)	MATRIX Bauer (2008) and tropospheric chemistry (Shindell et al., 2003)	No	No	NO	Distributed over all mixing states e.g. size distributions.	NASA GISS-E2, GCM, 2x2.5x40	Schmidt et al 2014
GISS OMA	EQSAM_v03d (Metastable ^b)	OMA (Bauer 2007) and tropospheric chemistry (Shindell et al., 2003)	Yes	No	Bauer and Koch, 2005	Fine mode	NASA GISS-E2, GCM, 2x2.5x40	Schmidt et al 2014
Oslo CTM2	EQSAM_v03d (Metastable)	Oslo CTM2 (Berntsen and Isaksen, 1997)	No	Yes	EQSAM_v03d	2 bins: fine and coarse mode	ECMWF, CTM, 2.8x2.8x60	Myhre et al., 2006
Oslo CTM3	EQSAM_v03d (Metastable)	Oslo CTM2 (Berntsen and Isaksen, 1997)	No	Yes	EQSAM_v03d	2 bins: fine and coarse mode	ECMWF, CTM, 2.25x2.25x60	Myhre et al., 2006

1236
1237
1238
1239
1240

^aStable state: where salts precipitate once the aqueous phase becomes saturated

^bMetastable: where the aerosol is composed only of a supersaturated aqueous phase

[CHEMDUSS: Chemistry reaction on dust and sea salt particles](#)

Formatted: Superscript

Table 2. Characteristics of thermodynamic equilibrium models

	ISORROPIA-I	ISORROPIA-II	MARS	RPMARES	INCA	EQSAM_v03d
Species	Sulfate, nitrate, ammonium, sodium, chloride	Sulfate, nitrate, ammonium, sodium, chloride, crustal species	Sulfate, nitrate, ammonium	Sulfate, nitrate, ammonium	Sulfate, nitrate, ammonium	Sulfate, nitrate, ammonium, sodium, chloride
# of components	23	34	16	11	9	18
# of reactions	15	27	7	6	4	25
Multicomponent activity coefficient	Bromley	Bromley	Bromley	Bromley	Seinfeld and Pandis	Metzger
Binary activity coefficient	Kusik and Meissner	Kusik and Meissner	Pitzer	Pitzer	Seinfeld and Pandis	Metzger
Water activity	ZSR ^a	ZSR	ZSR	ZSR		ZSR
Kelvin effect	No	No	No	No	No	No
Quantities that determine subdomains	[Na ⁺], [NH ₄ ⁺], [SO ₄ ²⁻]	[Ca ²⁺], [K ⁺], [Mg ²⁺], [Na ⁺], [NH ₄ ⁺], [SO ₄ ²⁻]	RH, [NH ₄ ⁺], [SO ₄ ²⁻]	[NH ₄ ⁺], [SO ₄ ²⁻]	[NH ₄ ⁺], [SO ₄ ²⁻]	[NH ₄ ⁺], [SO ₄ ²⁻]
# of subdomains	4	5	4	2	3	3

1241
1242
1243

^aZSR: Zdanovskii-Stokes-Robinson

Table3. Summary of the observational data used in this study

SURFACE NETWORK	QUANTITY	COVER AREA	# of sites in 2008	SAMPLE FREQUENCY	SOURCE
CASTNET	Concentration of HNO ₃ , NO ₃ ⁻ , NH ₄ ⁺ , SO ₄ ²⁻ Dry deposition of them	North America	83	weekly	www.epa.gov/castnet/clearsession.do
AMoN	Concentration of NH ₃	U.S.	19	2-weekly	http://nadp.isws.illinois.edu/

NADP/NTN	Wet deposition of HNO ₃ +NO ₃ ⁻ , NH ₄ ⁺ , SO ₄ ²⁻	U.S.	253	weekly	nadp.isws.illinois.edu
EMEP	Concentration of HNO ₃ , NH ₃ , NO ₃ ⁻ , NH ₄ ⁺ , SO ₄ ²⁻	Europe	35	daily	http://www.nilu.no/projects/ccc/index.html
EANET	Concentration of HNO ₃ , NH ₃ , NO ₃ ⁻ , NH ₄ ⁺ , SO ₄ ²⁻	East Asia	56	Daily to 2-weekly	http://www.eanet.asia/eanet/brief.html
	Wet deposition of HNO ₃ +NO ₃ ⁻ , NH ₄ ⁺ , SO ₄ ²⁻			24 hours or precipitation event	
AIRCRAFT CAMPAIGNS	QUANTITY	COVER AREA	# of Flights	CAMPAIGN PERIOD	SOURCE
ARCTAS-A	Concentration of NO ₃ ⁻ , NH ₄ ⁺ , SO ₄ ²⁻	Alaska, U.S.	11	March-April	http://www-air.larc.nasa.gov/cgi-bin/arcstat-c
ARCTAS-CARB		California Bay area U.S.	6	June	
ARCTAS-B		Central Canada	7	July	

1244
1245
1246

Table 4a. NO₃⁻ global budget for each model

Tracer	Model	Burden (Tg)	SConc (µg kg ⁻¹)	DDep (Tg a ⁻¹)	WDep (Tg a ⁻¹)	ChemDUSS ^a (Tg a ⁻¹)	ChemP ^a (Tg a ⁻¹)	Lifetime (days)	AOD ^b
NO ₃ ⁻	CHASER	0.16	0.18	-	-	-	-	-	0.0076
	EMAC	0.67	0.47	46.3	-	-	-	-	-
	EMEP	0.96	0.30	15.0	62.7	(71.7) ^c	4.5	0.0073	-
	GISS-MATRIX	0.22	0.06	1.3	9.6	(10.9)	7.4	-	-
	GISS-OMA	0.14	0.05	1.1	5.5	(6.6)	7.8	0.0153	-
	GMI	0.26	0.22	14.9	31.5	41.9	4.8	2.1	0.0047
	INCA	0.79	0.17	4.5	44.6	44.1	9.8	5.9	0.0064
	Oslo-CTM2	0.60	0.25	47.8	61.5	(109.3)	2.0	0.0018	-
	Oslo-CTM3	1.88	0.36	34.6	90.6	(125.2)	5.5	-	-
	Avg	0.63	0.23	20.7	45.9	60.6	5.0	0.0072	-
	Med	0.60	0.22	15.0	44.6	46.7	5.5	0.0064	-
Ratio ^d	13.4	9.4	43.5	16.5	19.0	3.9	8.5	-	

1247 ^a: ChemDUSS and ChemP refers to NO₃⁻ chemical production associated with
1248 dust/sea salt and NH₃/NH₄⁺, respectively
1249 ^b: AOD here includes NH₄⁺ that is associated to NO₃⁻ for all models except EMEP
1250 ^c: value inside parenthesis is estimated total NO₃⁻ chemical production based on its
1251 total loss, while budget without parenthesis is reported directly by model.
1252 ^d: a ratio between maximum to minimum model simulations
1253
1254
1255

Table 4b NH₃ and NH₄⁺ global budget for each model

Tracer	Model	Emi (Tg a ⁻¹)	Burden (Tg)	SConc (µg kg ⁻¹)	DDep (Tg a ⁻¹)	WDep (Tg a ⁻¹)	ChemP/L ^a (Tg a ⁻¹)	Lifetime (days)	AOD
NH ₄ ⁺	CHASER	0.75	0.44	20.9	7.2	(28.1) ^{ba}	9.8	-	-
	EMAC	0.19	0.12	3.6	44.5 ^{cb}	-	-	-	-
	EMEP	0.20	0.15	4.0	26.4	(30.4)	2.4	0.0059	-
	GISS-MATRIX	0.31	0.18	4.1	27.9	(32.0)	3.5	-	-
	GISS-OMA	0.31	0.19	4.2	24.0	(28.2)	4.0	-	-
	GMI	0.17	0.14	1.7	30.6	32.2	1.9	-	-
	INCA	0.39	0.08	2.4	20.4	22.9	6.3	-	-

Formatted: Superscript

	Oslo-CTM2	0.29	0.14	5.3	32.6	(37.9)	2.8	-
	Oslo-CTM3	0.30	0.16	5.6	26.1	(31.7)	3.5	-
	Avg	0.32	0.18	5.8	24.4 ^{d,e}	30.4	4.3	
	Med	0.30	0.15	4.1	26.3 ^{d,e}	31.1	3.5	
	Ratio	4.4	5.5	12.3	4.5 ^c	1.7	5.2	
NH ₃	CHASER	62.8	0.13	0.46	19.8	6.8	(36.2) ^{b,a}	0.76
	EMAC	59.3	0.85	1.39	15.5	-	-	-
	EMEP	56.9	0.09	0.46	15.4	18.2	(33.6)	0.98
	GISS-MATRIX	63.4 ^{e,d}	0.17	0.26	18.1	13.4	(31.9)	0.98
	GISS-OMA	63.4 ^{e,d}	0.17	0.25	18.4	16.7	(28.3)	0.98
	GMI	60.4	0.11	0.40	12.6	17.5	30.4	0.67
	INCA	70.5 ^{e,d}	0.12	0.39	29.3	18.6	22.4	0.62
	Oslo-CTM2	65.9	0.08	0.27	15.8	8.1	(42.0)	0.44
	Oslo-CTM3	63.3	0.05	0.51	23.7	7.7	(31.9)	0.29
	Avg	62.9	0.20	0.49	18.7	13.4	32.1	0.72
	Med	63.3	0.12	0.40	18.1	15.1	31.9	0.72
	Ratio	1.2	17.0	5.6	2.3	2.7	1.9	3.4

- 1256 ^aChemP/L: chemical production or loss term
1257 ^{b,a} chemical budgets inside parenthesis are inferred based on the reported emission
1258 and total deposition
1259 ^{c,b} EMAC gives total wet deposition of NH₄⁺ and NH₃
1260 ^{d,e} Statistic values of NH₄⁺ wet deposition do not include EMAC
1261 ^{e,d} INCA uses ECLIPSE anthropogenic emissions, two GISS models use CMIP5
1262 anthropogenic emission, and all other models use HTAPv2 anthropogenic emissions
1263
1264

Formatted: Not Superscript/ Subscript

Table 4c. HNO₃ global budget for each model

Tracer	Model	Burden ^a (Tg)	SConc (µg kg ⁻¹)	DDep (Tg a ⁻¹)	WDep (Tg a ⁻¹)	CheAP ^b (Tg a ⁻¹)	CheGP ^c (Tg a ⁻¹)	CheAL ^d (Tg a ⁻¹)	CheGL ^e (Tg a ⁻¹)	Lifetime (days)
HNO ₃	CHASER	1.1	0.29	74.0 ^{f,a}	120.9 ^{f,b}	-	-	-	-	-
	EMAC	3.1	0.32	56.1	136.0 ^{f,b}	-	-	-	-	-
	EMEP	0.66	0.04	39.2	123.9	-	-	-	-	-
	GISS-MATRIX	5.7	0.12	61.7	167.5	-	-	-	-	-
	GISS-OMA	5.3	0.10	49.8	148.2	-	-	-	-	-
	GMI	1.8	0.18	39.7	128.1	128.1	413	42.6	299	3.5
	INCA	1.5	0.09	47.7	77.5	21	369	10.0	210	5.7
	Oslo-CTM2	1.3	0.05	36.1	66.0	-	-	-	-	-
	Oslo-CTM3	2.3	0.04	36.0	49.3	-	-	-	-	-
	Avg	2.5	0.14	45.8 ^{f,b}	108.7 ^{f,e}	-	-	-	-	-
	Med	1.8	0.10	43.7 ^{f,b}	123.9 ^{f,e}	-	-	-	-	-
	Ratio	8.6	8.0	1.6 ^b	3.4 ^b	-	-	-	-	-

- 1265 ^aHNO₃ burden for the atmosphere up to 100 hPa
1266 ^bCheAP: chemistry production from aerosol phase
1267 ^cCheGP: chemistry production from gas phase
1268 ^dCheAL: chemistry loss from aerosol phase
1269 ^eCheGL: chemistry loss from gas phase
1270 ^{f,b} for both HNO₃ and NO₃

Formatted: Superscript

Formatted: Superscript

Formatted: Superscript

Formatted: Superscript

Formatted: Superscript

Formatted: Superscript

Formatted: Superscript

Formatted: Superscript

1271 ^cstatistical values do not include CHASER and EMAC that report total dry or wet
 1272 deposition of HNO₃ and NO₃⁻

1273

1274 **Table 4d. SO₄²⁻ global budget for each model**

Tracer	Model	Emi SO ₂ (Tg a ⁻¹)	Emi SO ₄ (Tg a ⁻¹)	Burden (Tg)	SConc (µg kg ⁻¹)	DDep (Tg a ⁻¹)	WDep (Tg a ⁻¹)	Chem GP ^a (Tg a ⁻¹)	Chem AqP ^b (Tg a ⁻¹)	Lifetime (days)	AOD
SO ₄ ²⁻	CHASER	111	0	3.3	1.44	22.1	137	(159)		7.6	0.0826
	EMAC	138	619 ^{ca}	1.9	1.72	504 ^{db}	302	(187)		0.86	-
	EMEP	109	0	0.83	0.45	10.2	109	(119)		2.5	0.0232
	GISS-MATRIX	133	5.1	1.3	0.63	16.6	97	(109)		4.2	-
	GISS-OMA	133	5.1	1.1	0.53	11.8	112	52.7	66.2	3.3	0.0714
	GMI	111	0	1.1	0.58	7.5	205	126.5	86.1	3.6	0.0257
	INCA	116	8.0	1.8	0.34	8.4	116	42.2	75.1	5.3	0.0417
	Oslo-CTM2	133	4.1	2.0	0.49	17.6	184	(198)		3.6	0.0366
	Oslo-CTM3	133	4.1	2.7	0.55	20.2	160	(176)		5.5	
	Avg ^{de}	122		1.8	0.63	14.3	140		151	4.5	0.0469
	Med ^{de}	133		1.6	0.54	14.2	127		139	3.9	0.0392
	Ratio ^{de}	1.2		4.0	4.2	2.9	2.1		2.0	3.0	3.6

Formatted: Superscript

Formatted: Superscript

1275 ^a ChemGP: Chemistry production from gas phase reaction

1276 ^b ChemAqP: Chemistry production from aqueous phase reaction

1277 ^{ca} EMAC emission also includes sea spray SO₄²⁻

1278 ^{db} EMAC dry deposition includes sedimentation and SO₄²⁻ sedimentation is very high
 1279 since it has assumed that 7.7% of sea salt is SO₄²⁻

1280 ^{de} Statistical values do not include EMAC

1281

1282 **Table 5: Effective Henry Law constant used in the models**

Aerocom Model	H ⁰ (M/atm)	-ΔH _{sol} /R (K)
CHASER	3.0e+5	3400
EMAC ^a	-	-
EMEP ^b	-	-
GIS MATRIX	1.e+2	3415
GISS OMA	1.e+2	3415
GMI	1.05e6	4200
INCA	7.4e+1	3400
Oslo-CTM2	3.3e+6	0
Oslo-CTM3	3.3e+6	0

Formatted: Not Superscript/ Subscript

Formatted: Not Superscript/ Subscript

1283 ^aEMAC: See its wet deposition description in section 4.1.1.

1284 ^bEMEP: The model does not use Henry law but applies simple empirical scavenging
 1285 ratio, which for NH₃ is 1.4e6 for in-cloud and 0.5e6 for below-cloud scavenging. The
 1286 scavenging ratio by definition is the ratio the concentration of a certain pollutant in
 1287 precipitation divided by the concentration of the pollutant in air.

1288

1289

1290

1291

1292 **Table 6. Baseline and three sensitivity experiments in the GMI model**

Experiment	Setup	Purpose
BASE	Standard simulation as described in section 2.1	Baseline simulation
TWET	Set NH ₃ effective Henry law constant from 1.05e+6 (pH= 5.0) to 62 (pure water)	Review impact of NH ₃ wet deposition
TnoNH3	Turn off NO ₃ ⁻ production from NH ₃ /NH ₄ ⁺	Identify how large/where the NO ₃ ⁻ formation from NH ₃ /NH ₄ ⁺
TnoHET	Turn off NO ₃ ⁻ production from dust and sea salt	Identify how large/where the NO ₃ ⁻ formation from dust and sea salt

1293
1294 **Table 7: NO₃⁻, NH₄⁺, NH₃ and HNO₃ budgets from the base simulation and three**
1295 **sensitivity experiments**

Tracer	Exps	Burden (Tg)	SConc (µg kg ⁻¹)	DDep (Tg a ⁻¹)	WDep (Tg a ⁻¹)	ChemDUSS (Tg a ⁻¹)	ChemP((Tg a ⁻¹)	Lifetime (days)
NO ₃ ⁻	BASE	0.26	0.22	14.9	31.5	41.9	4.8	2.1
	Twet	0.97	0.23	14.8	43.3	41.0	18.3	6.0
	TnoNH3	0.20	0.17	14.7	27.5	42.3	0	1.7
	TnoHET	0.099	0.065	0.61	6.70	0	7.1	5.0

1296

Tracer	Model	Emi (Tg a ⁻¹)	Burden (Tg)	SConc (µg kg ⁻¹)	DDep (Tg a ⁻¹)	WDep (Tg a ⁻¹)	ChemP/L (Tg a ⁻¹)	Lifetime (days)
NH ₄ ⁺	BASE		0.17	0.14	1.7	30.6	32.2	1.9
	Twet		0.48	0.16	1.9	50.7	53.0	3.4
	TnoNH3		-	-	-	-	-	-
	TnoHET		0.17	0.14	1.6	30.6	32.2	1.9
NH ₃	BASE	60.4	0.11	0.40	12.6	17.5	30.4	0.67
	Twet		0.85	0.81	8.70	1.1	50.1	5.2
	TnoNH3		0.32	0.58	20.9	39.3	0	1.9
	TnoHET		0.10	0.40	12.6	17.4	30.4	1.2

1297
1298
1299

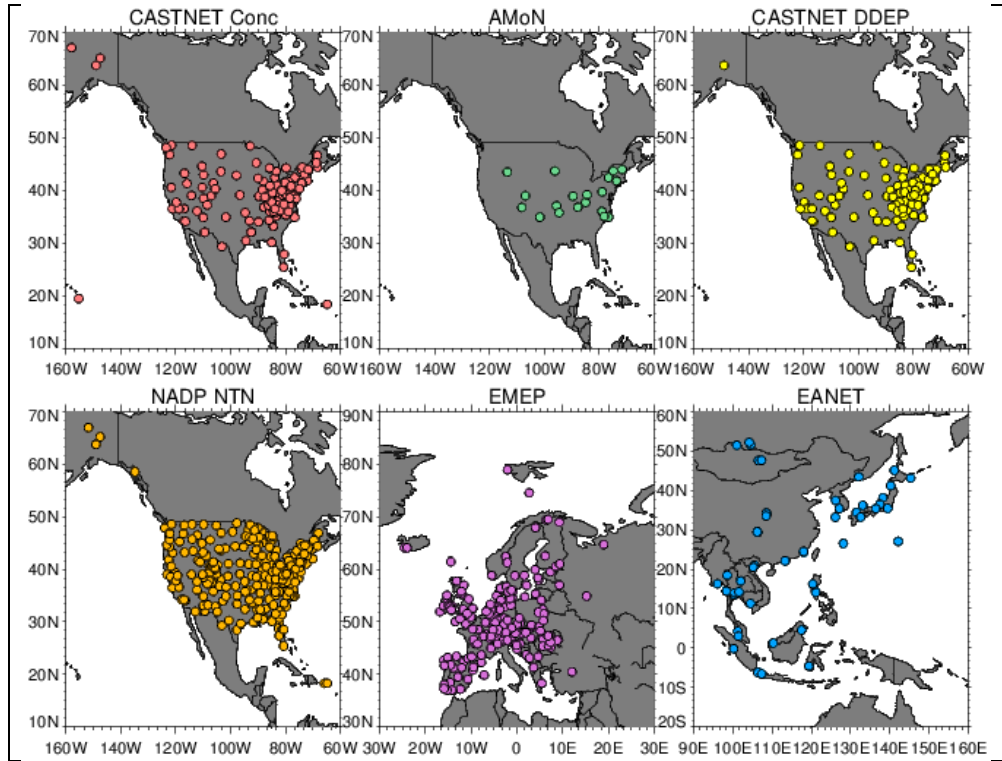


Figure 1. The observational station locations for CASTNET surface concentrations (CASTNET Conc), Ammonia surface monitor network over U.S. (AMON), CASTNET dry deposition (CASTNET DDEP); National Acid Deposition Network for wet deposition over U.S. (NADP NTN), surface concentrations over Europe (EMEP), and surface dry and wet deposition over Asia (EANET).

1300
1301
1302

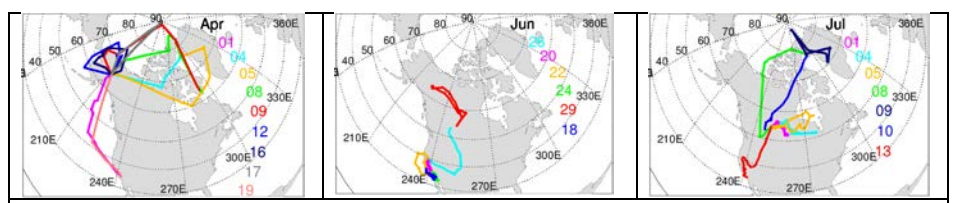


Figure 2. Flight-tracks of ARTCTA-A (left), ARCTAS-CARB (middle), and ARCTAS-B (right). The colors represent observations during different days.

1303